Molecular dynamics simulations of radiation damage and recovery in high temperature superconductors

IRradiation Effects on HTS for Fusion – Arona, Italy, Nov 2023

R. Gray, M. Sanjeev, A. Dickson and S. T. Murphy (samuel.murphy@lancaster.ac.uk)

Radiation damage in HTS materials

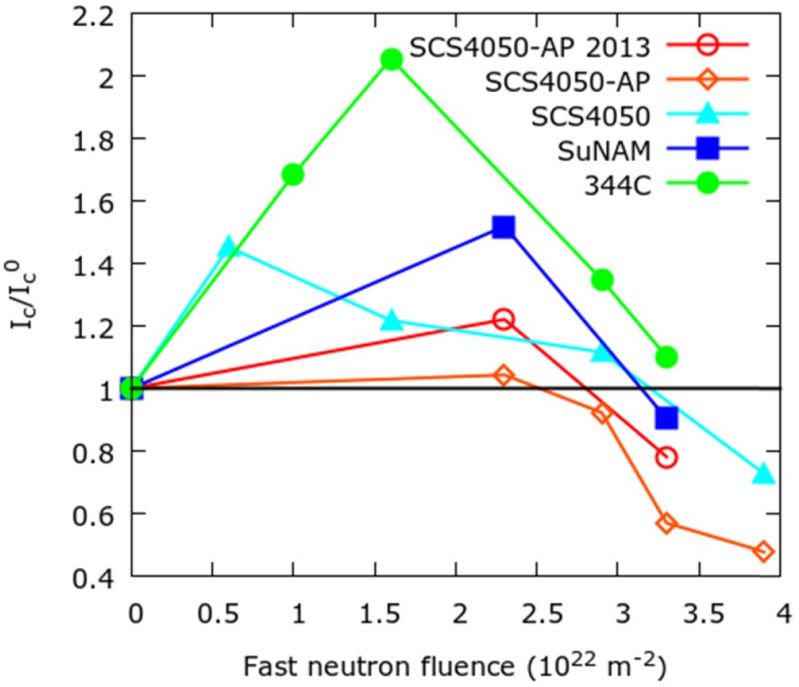

Fig 1: Plot showing how the critical current of different superconducting tapes changes as a function of neutron fluence (Fischer *et al*. SUST 31 (2018) 044006).

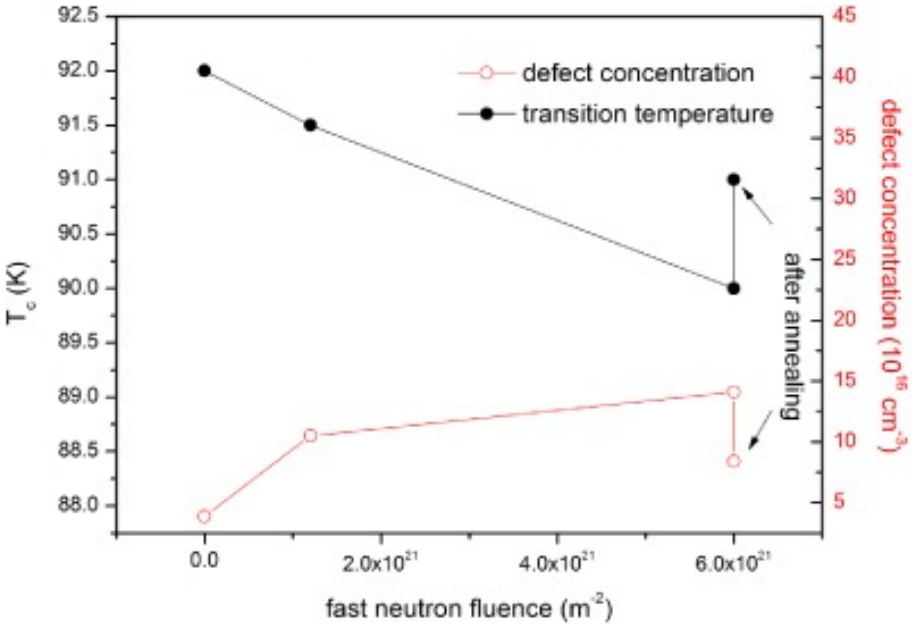

Fig 2: Plot showing the decrease of Tc a function of neutron fluence (Chudy *et al*. SUST 25 (2012) 075017).

TEM observation of a cascade

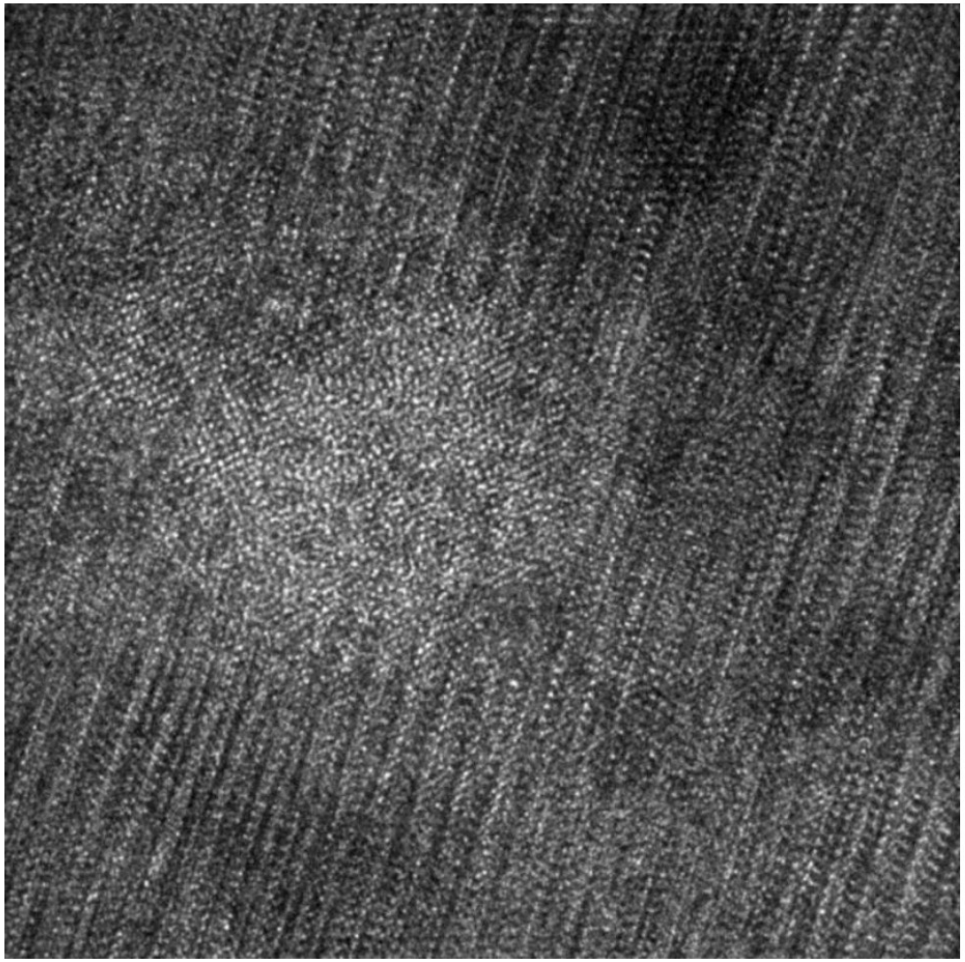

Fig 3: High resolution TEM image of cascade damage in HTS (Oxford).

Radiation damage in HTS materials

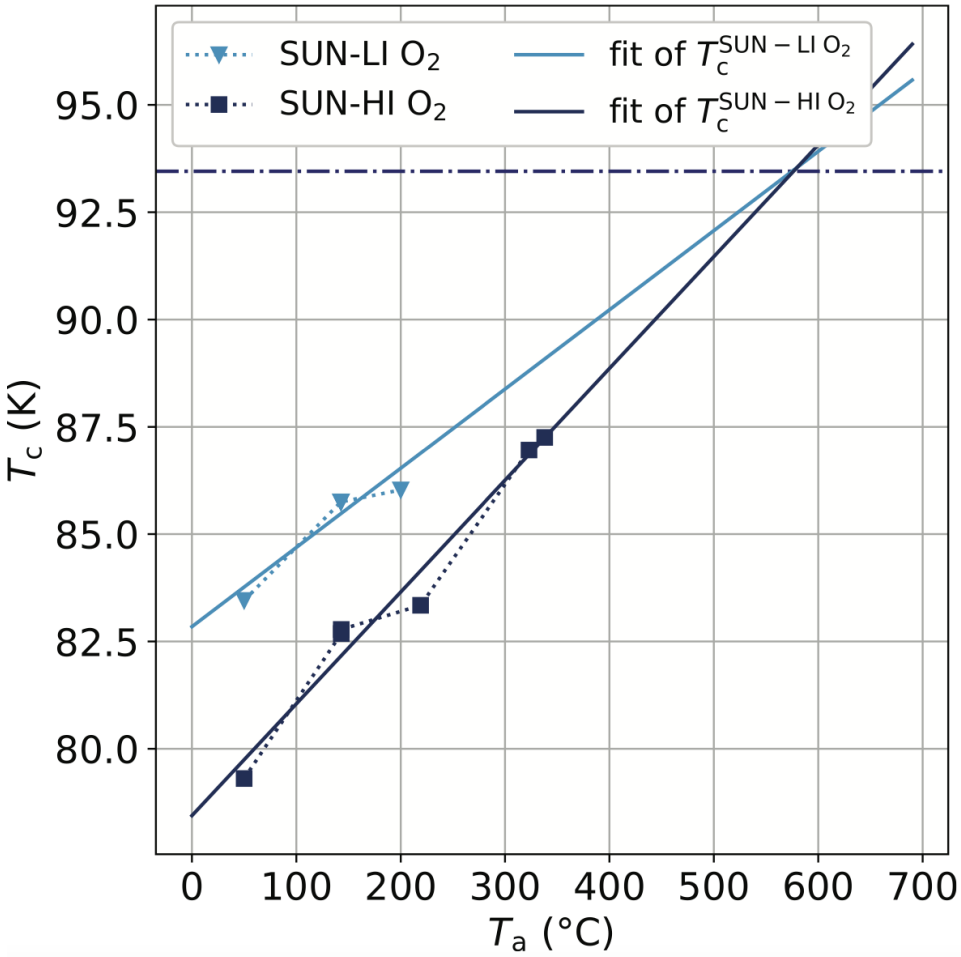

Fig 4: Recovery of the critical temperature as a function of annealing temperature (Unterrainer *et al*. SUST 35 (2022) 04LT01).

There is a general consensus that there is some recovery of superconducting properties upon annealing.

The radiation damage process

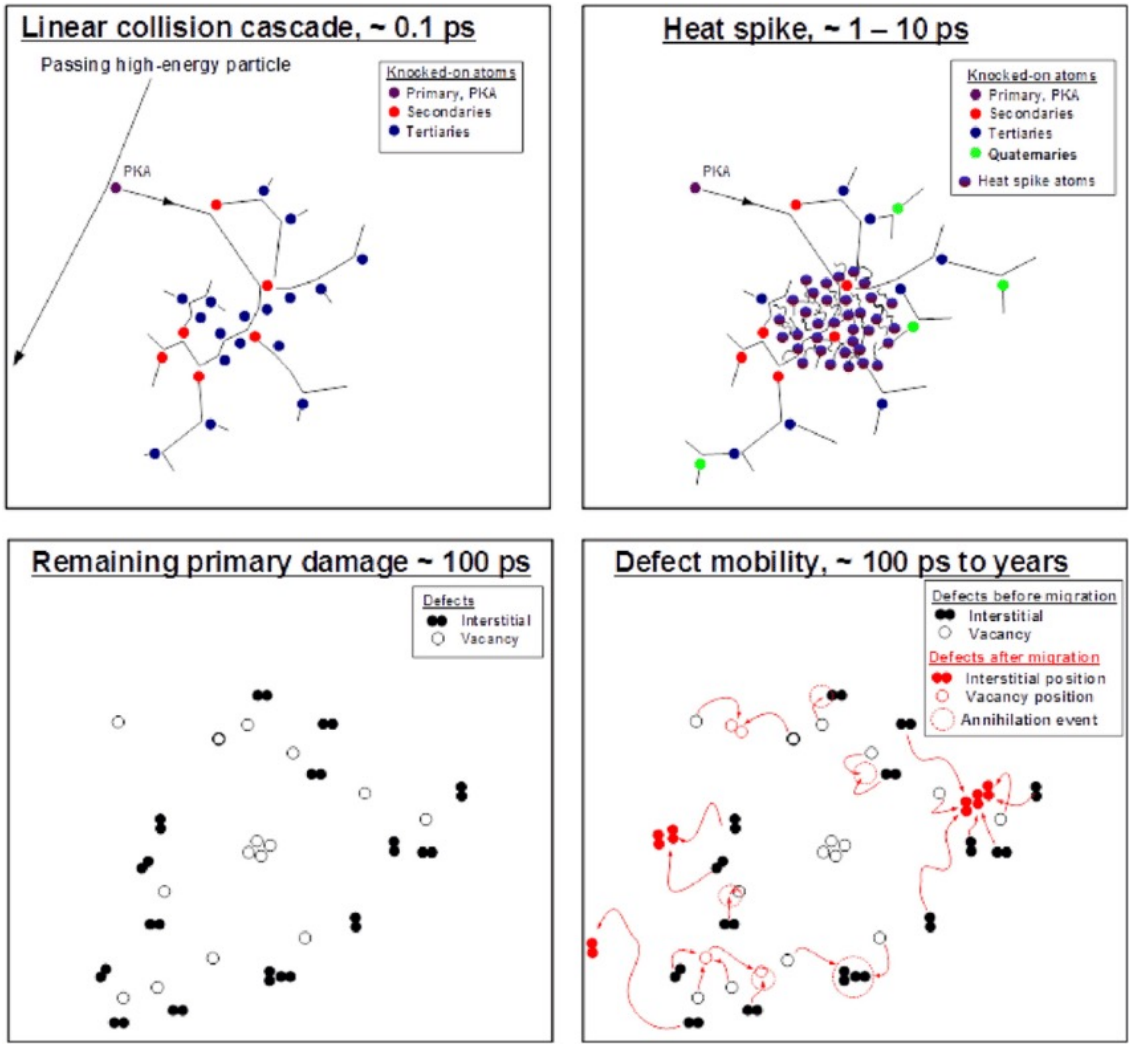

Fig 5: An schematic of the irradiation damage process (Nordlund *et al*. J. Nucl. Mater. 512 (2018) 450).

The multiscale modelling approach

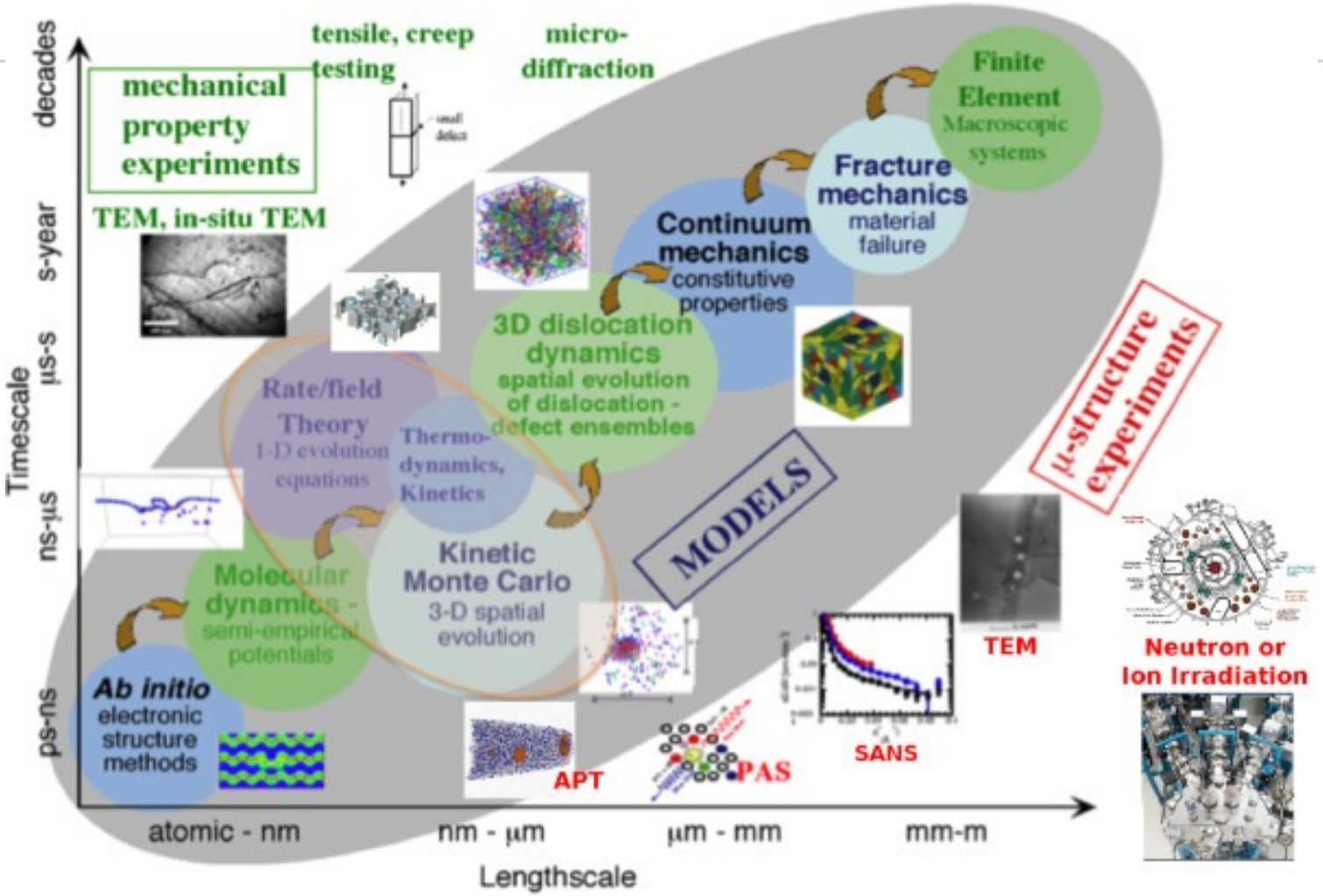

Fig 6: The multiscale modelling approach for fusion (Gilbert *et al*. J. Nucl. Mater. 554 (2021) 153113.

Crystal structure of $YBa_2Cu_3O_7$

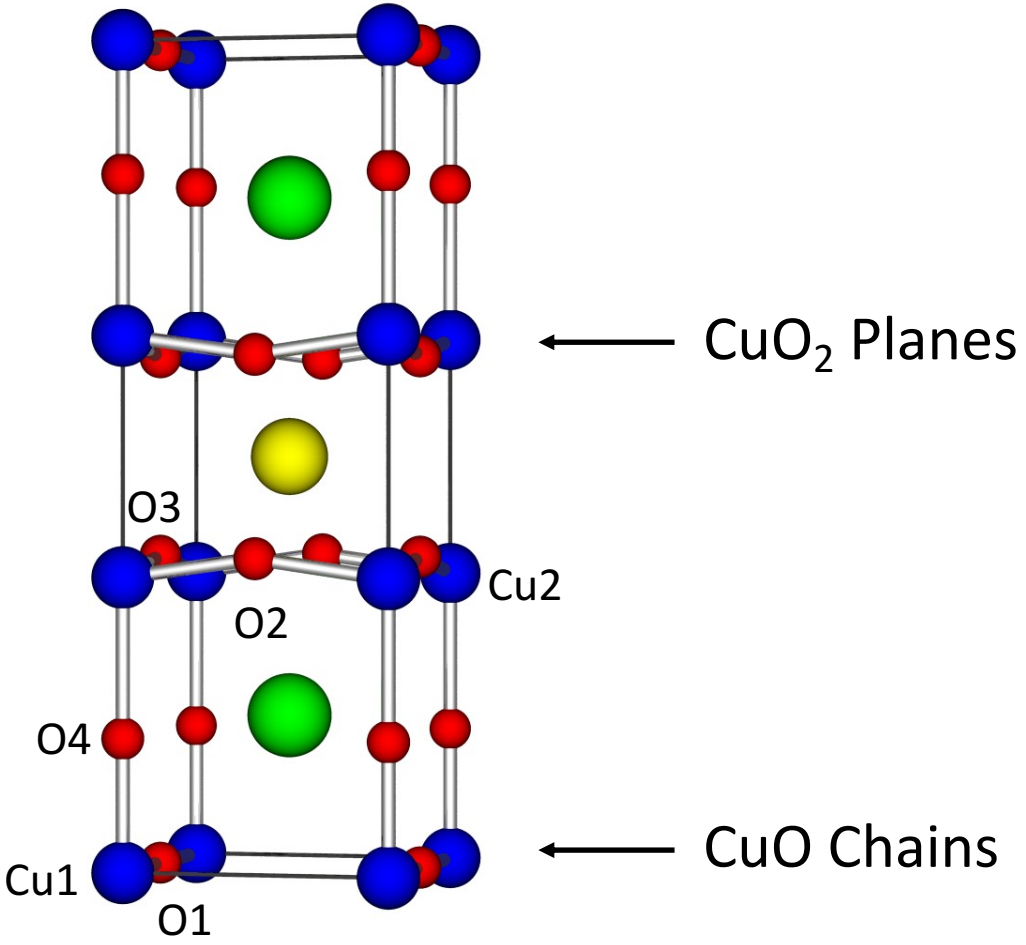

Fig 7: Crystal structure of $YBa_2Cu_3O_7$.

Early atomistic simulation of HTS materials

- The first atomistic simulations of HTS appeared very early on.

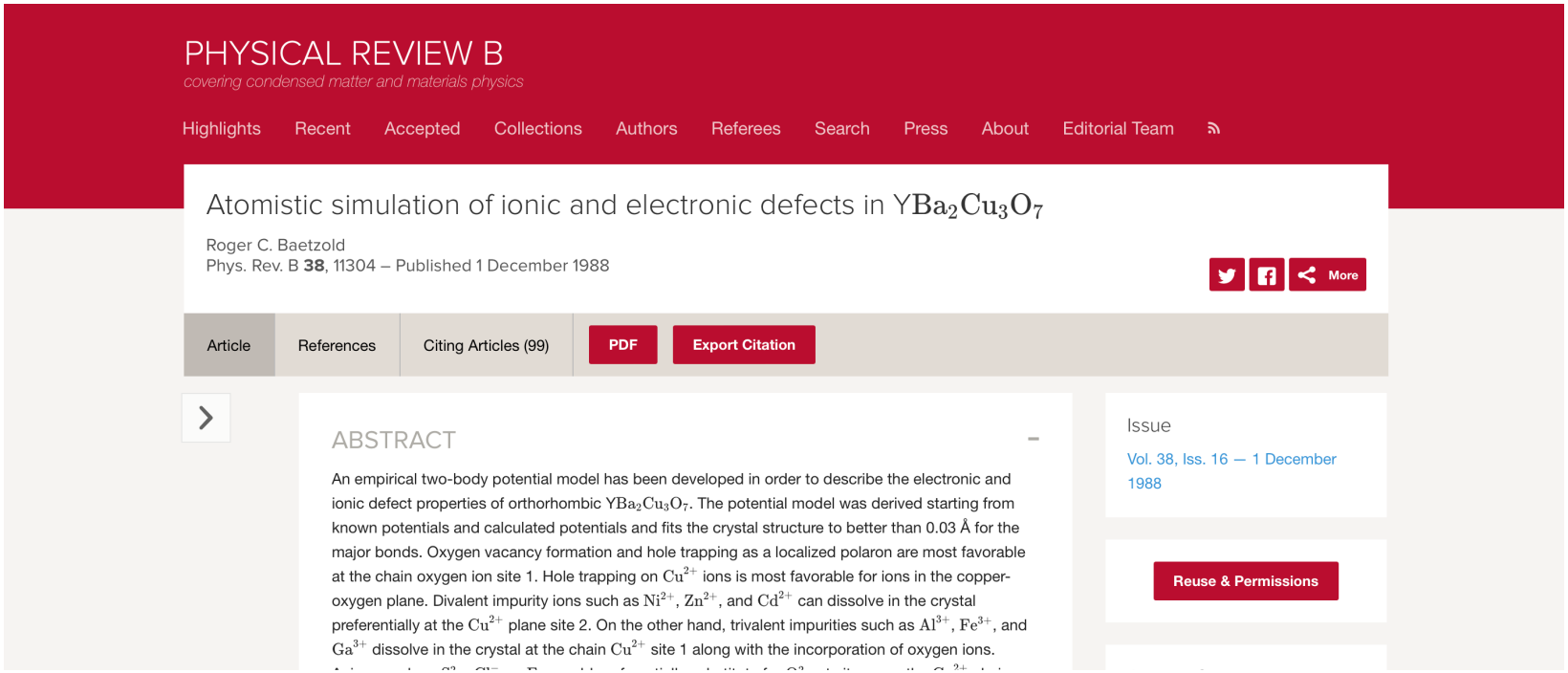

PHYSICAL REVIEW B

covering condensed matter and materials physics

Highlights Recent Accepted Collections Authors Referees Search Press About Editorial Team

Atomistic simulation of ionic and electronic defects in $YBa_2Cu_3O_7$

Roger C. Baetzold
Phys. Rev. B **38**, 11304 – Published 1 December 1988

More

Article References Citing Articles (99) PDF Export Citation

ABSTRACT

An empirical two-body potential model has been developed in order to describe the electronic and ionic defect properties of orthorhombic $YBa_2Cu_3O_7$. The potential model was derived starting from known potentials and calculated potentials and fits the crystal structure to better than 0.03 Å for the major bonds. Oxygen vacancy formation and hole trapping as a localized polaron are most favorable at the chain oxygen ion site 1. Hole trapping on Cu^{2+} ions is most favorable for ions in the copper-oxygen plane. Divalent impurity ions such as Ni^{2+}, Zn^{2+}, and Cd^{2+} can dissolve in the crystal preferentially at the Cu^{2+} plane site 2. On the other hand, trivalent impurities such as Al^{3+}, Fe^{3+}, and Ga^{3+} dissolve in the crystal at the chain Cu^{2+} site 1 along with the incorporation of oxygen ions.

Issue
Vol. 38, Iss. 16 — 1 December 1988

Reuse & Permissions

Fig 8: An early paper on atomistic simulation of $YBa_2Cu_3O_7$ (Baetzold, Phys. Rev. B 38 (1988) 11304.

Point defects in $YBa_2Cu_3O_7$ from DFT

Lancaster University

- Determine defect formation energies using DFT in the CASTEP code
  - Simulation parameters
  - GGA functional (PBE)
  - Ultrasoft pseudopotential with a cutoff of 600 eV
  - k-points 8x8x4 in the unitcell
  - Defect calculations in 4x4x1 supercell
  - Volume kept constant during defect simulation

Lattice parameters and elastic constants

	DFT	Lit
a /Å	3.840	3.821
b /Å	3.919	3.884
c /Å	11.830	11.677
C_{11} /GPa	215.97	211-234
C_{12} /GPa	109.24	37-132
C_{13} /GPa	58.03	71-100
C_{22} /GPa	232.40	230-268
C_{33} /GPa	142.55	138-186
C_{44} /GPa	51.13	35-61
C_{55} /GPa	41.19	33-50
C_{66} /GPa	81.72	57-97

Vacancy defects in $YBa_2Cu_3O_7$

Formation energies for vacancy defects in eV

Defect	Rich	Poor
V_Y	10.82	-12.49
V_{Ba}	7.17	-4.51
V_{Cu1}	2.15	-5.63
V_{Cu2}	1.76	-6.03
V_{O1}	1.01	-2.33
V_{O2}	1.6	-1.74
V_{O3}	1.71	-1.62
V_{O4}	0.88	-2.45

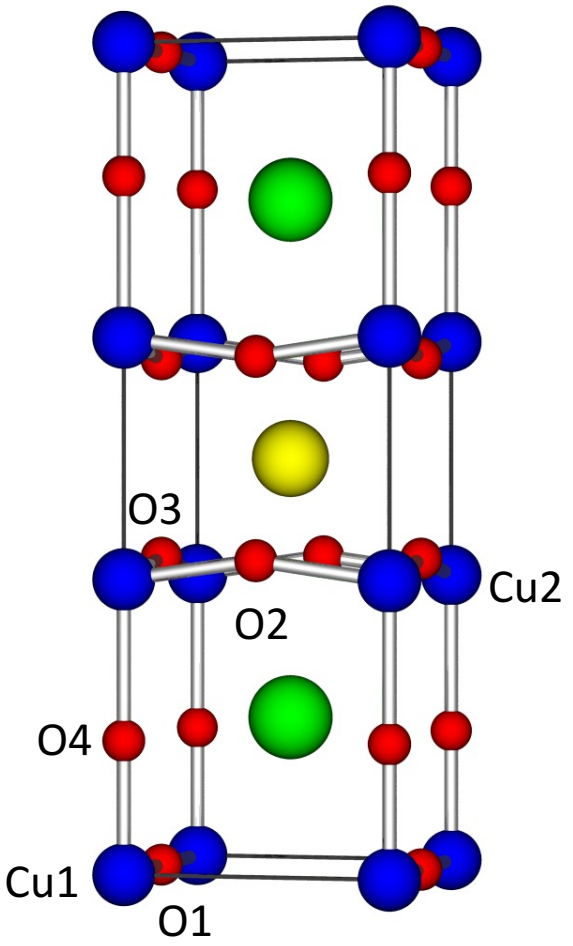

Fig 9: Crystal structure of $YBa_2Cu_3O_7$.

Antisite defects in $YBa_2Cu_3O_7$

Formation energies for antisite defects in eV

Defect	Rich	Poor
Ba_Y	4.34	-7.34
Y_{Ba}	-2.81	8.87
Ba_{Cu1}	-1.56	2.34
Ba_{Cu2}	-0.63	3.27
Cu_{Ba}	5.70	1.80
Cu_Y	9.55	-6.03
Y_{Cu1}	4.97	10.60
Y_{Cu2}	-6.17	9.41

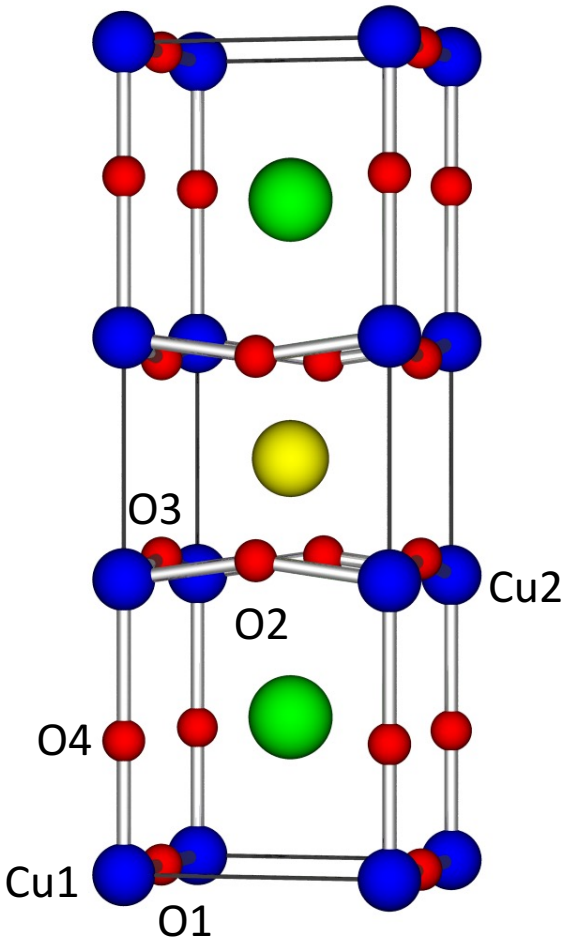

Fig 10: Crystal structure of $YBa_2Cu_3O_7$.

Interstitial defects in $YBa_2Cu_3O_7$

Lancaster University

Formation energies for interstitial defects in eV. All chemical potentials are in the rich state.

Site	O	Y	Ba	Cu
1	2.44	-0.31	1.84	1.52
2	0.26	**-1.94**	**0.55**	2.60
3	2.27	-1.61	2.73	**1.33**
4	0.27	-1.31	0.55	1.81
5	**0.1**	-1.63	3.06	2.91
6	**0.1**	1.65	3.89	2.49
7	**0.1**	3.01	5.55	3.27

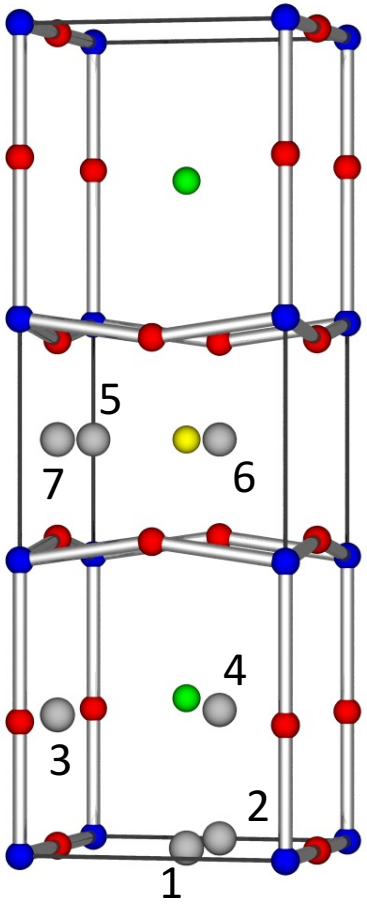

Fig 11: Interstitial sites in $YBa_2Cu_3O_7$.

Intrinsic defect processes

Lancaster University

Reaction energies for the intrinsic defect processes in $YBa_2Cu_3O_7$ (Normalised per defect)

Reaction	Energy /eV
$O_O \rightarrow O_i + V_O$	0.49
$Y_Y \rightarrow Y_i + V_Y$	4.46
$Ba_{Ba} \rightarrow Ba_i + V_{Ba}$	3.86
$Cu_{Cu} \rightarrow Cu_i + Cu_Y$	3.08
$Y_Y + 2Ba_{Ba} + 3Cu_{Cu} + \rightarrow V_Y + 2V_{Ba} + 3V_{Cu} + 7V_O + YBa_2Cu_3O_7$	1.02
$Y_Y + Ba_{Ba} \rightarrow Ba_Y + Y_{Ba}$	0.76
$Y_Y + Cu_{Cu} \rightarrow Cu_Y + Y_{Cu}$	1.69
$Cu_{Cu} + Ba_{Ba} \rightarrow Ba_{Cu} + Cu_{Ba}$	2.07

Oxygen vacancy clustering

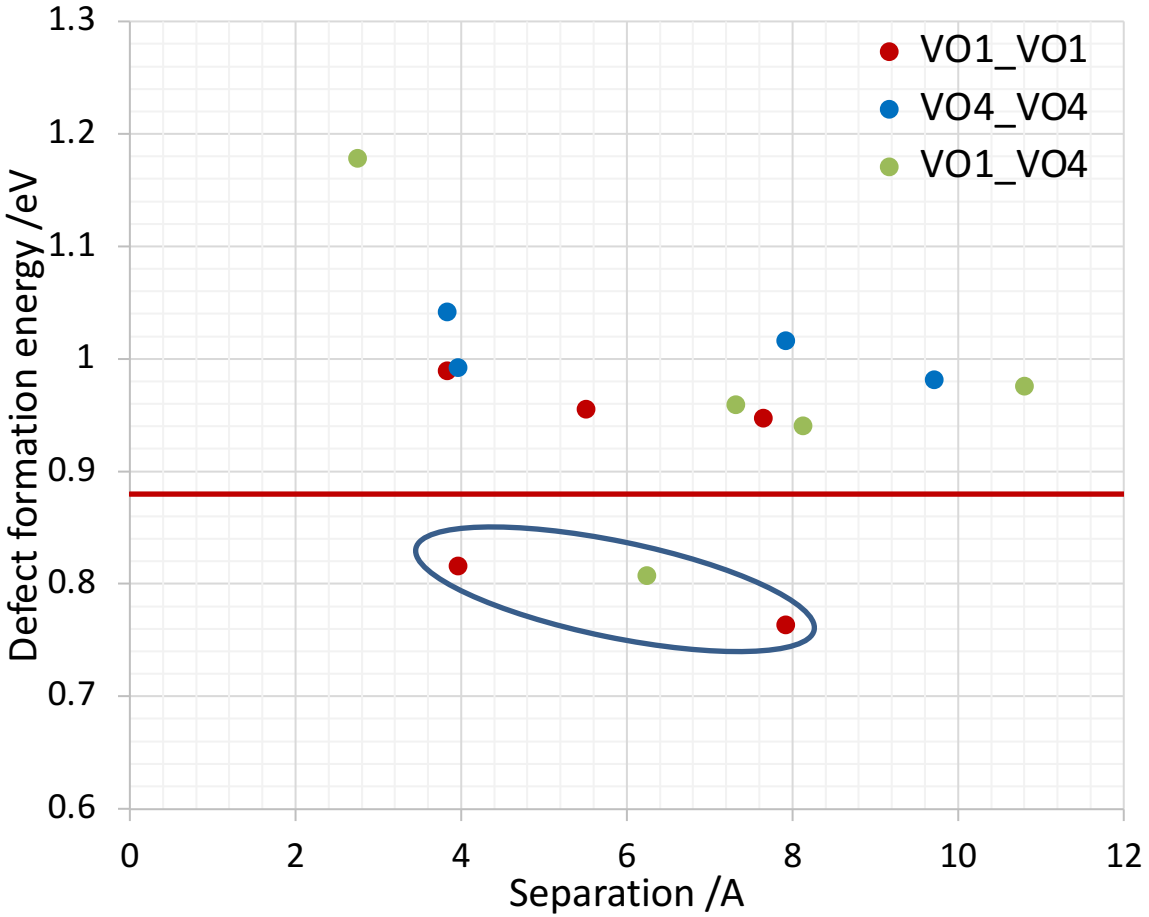

Fig 12: Plot showing the defect formation energy per oxygen vacancy for binary V_O clusters in $YBa_2Cu_3O_7$.

Oxygen vacancy clustering

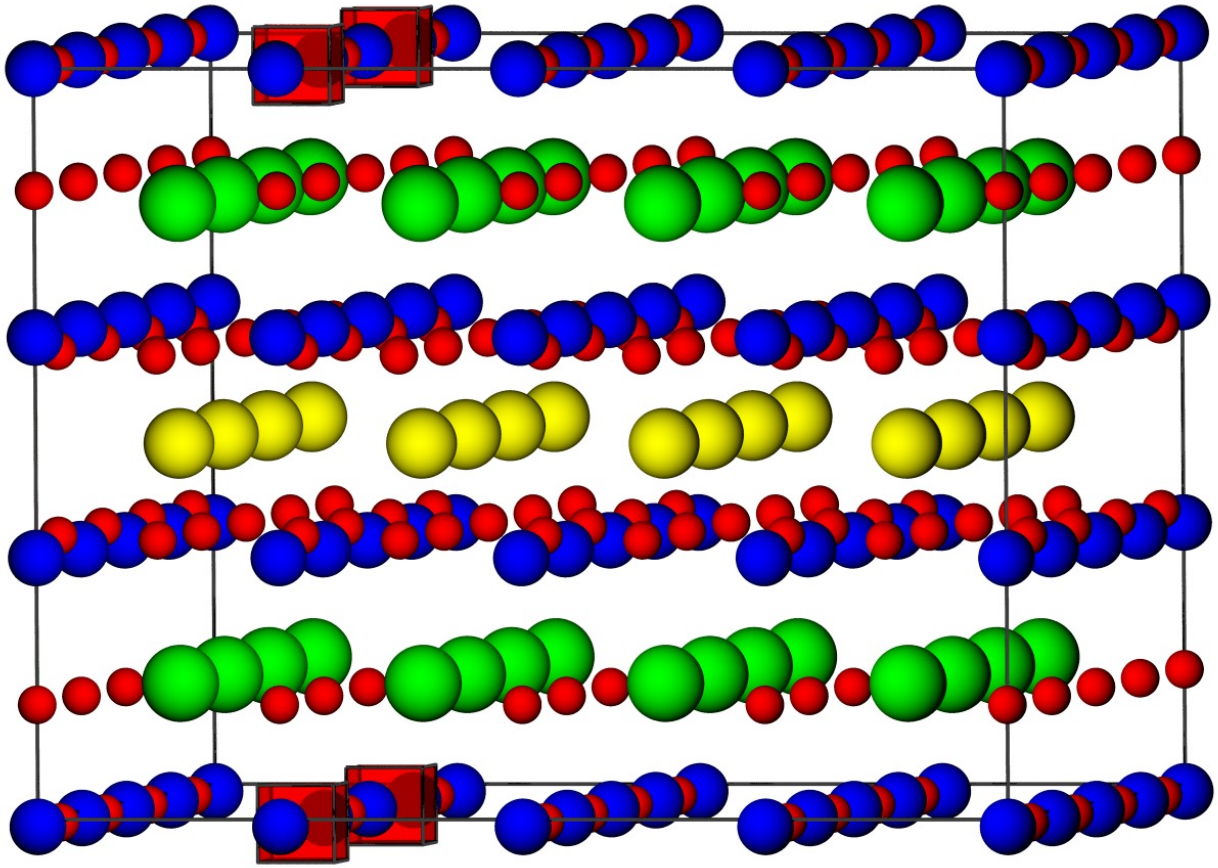

Fig 13: Simulation supercell showing the positions of lowest energy V_O clusters in $YBa_2Cu_3O_7$.

Point defect model – Cu-poor conditions

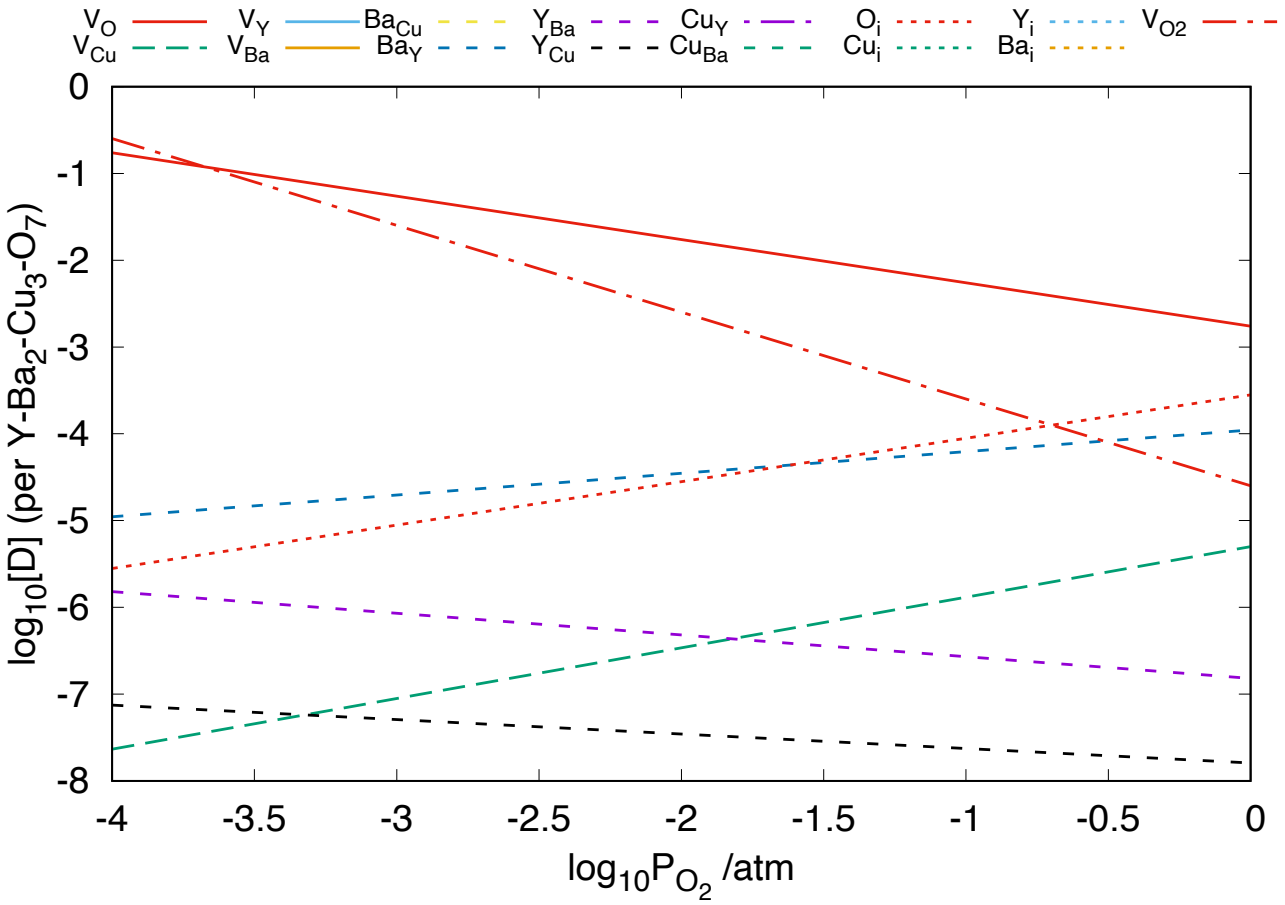

Fig 14: Brouwer diagram showing the defect chemistry of $YBa_2Cu_3O_7$ under Cu-poor conditions at 700 K.

Point defect model – Cu-poor conditions

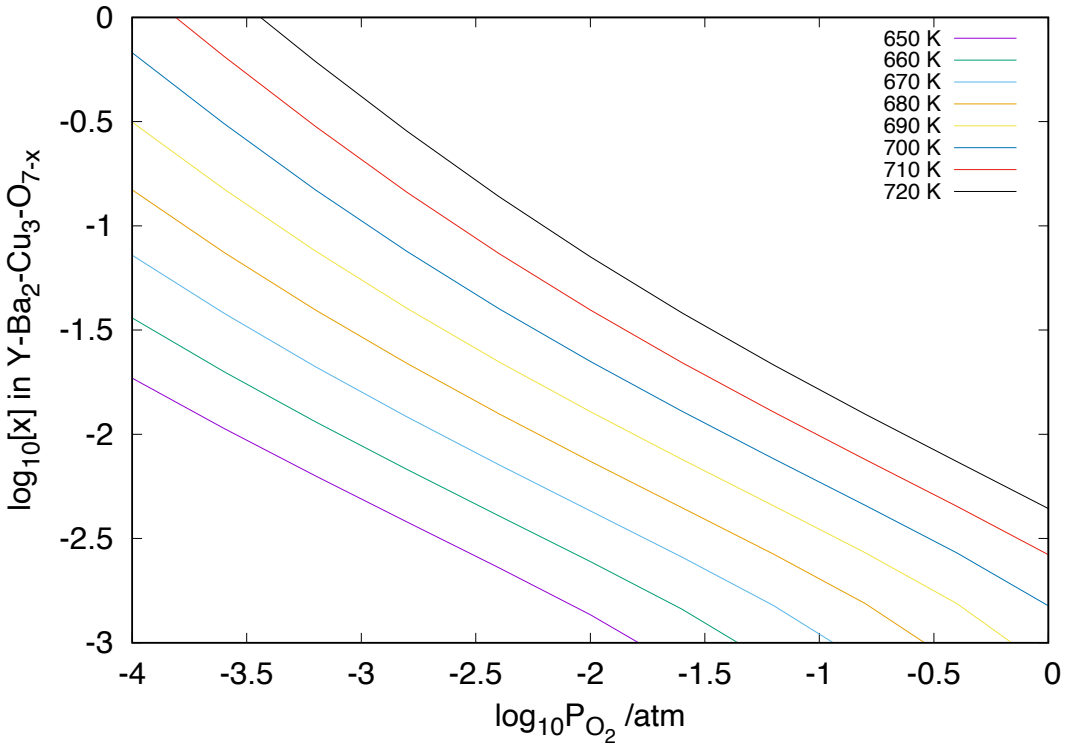

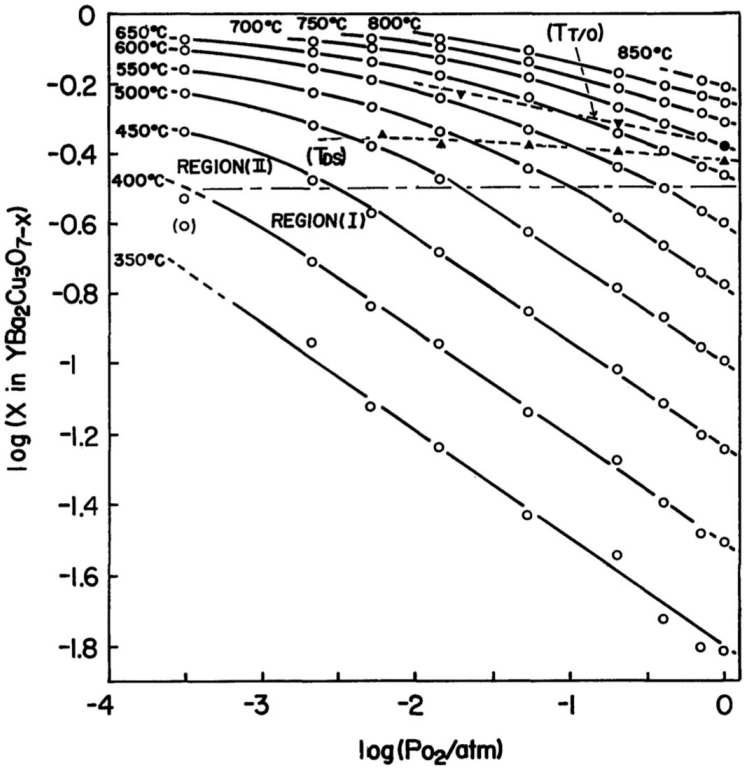

Fig 15: Plot showing how the oxygen stoichiometry variers with oxygen partial pressure and temperature compared to experiment of Yamaguchi *et al*. J. Appl. Phys. 27 (1988) L179.

Simulation of radiation damage using molecular dynamics

- Use Newton's equations of motion to evolve atoms in time, i.e.:

$$F = ma$$

- To represent transfer of energy from a neutron rescale velocity of primary knock-on atom (pka).
- Advantages
  - Atomic level insight
  - Includes recombination
  - Can control temperature

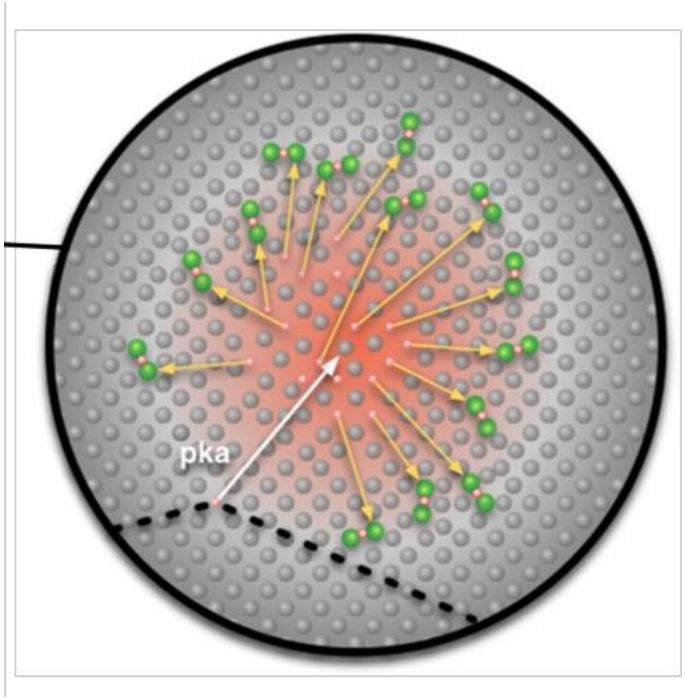

Fig 16: Illustration of a displacement cascade.

Empirical potential

- Need a potential model to describe the interactions between ions.

$$E^{Coul} = \frac{q_i q_j}{4\pi\varepsilon_0 r} \ldots.$$

$$+A\, exp\left(-\frac{r}{\rho}\right) - \frac{C}{r^6}$$

- Where, q_i and q_j are the charges on the ions and A, ρ and C are potential parameters that need to be derived.

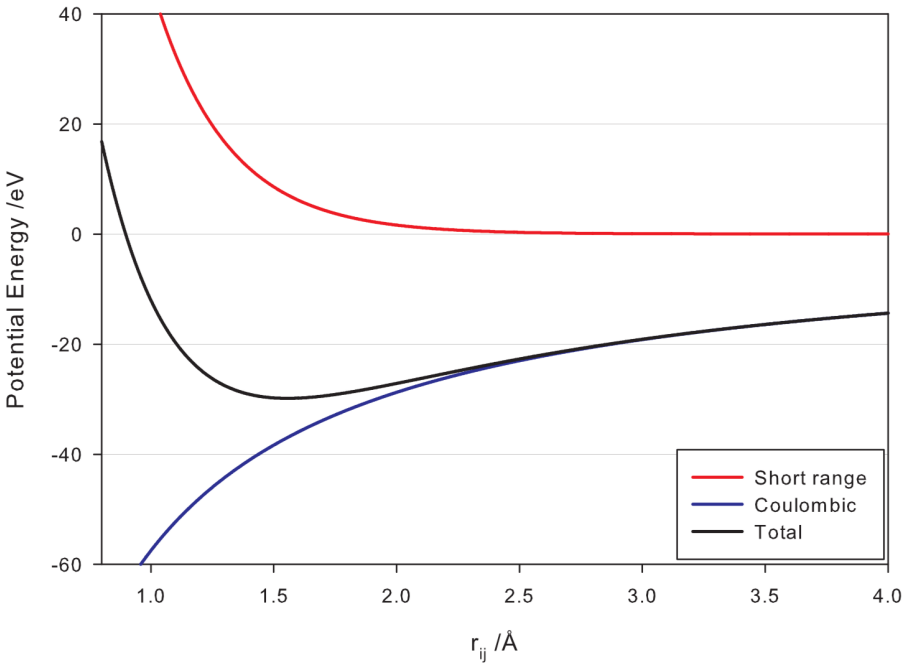

Fig 17: A typical Buckingham potential.

Previous cascades in $YBa_2Cu_3O_7$

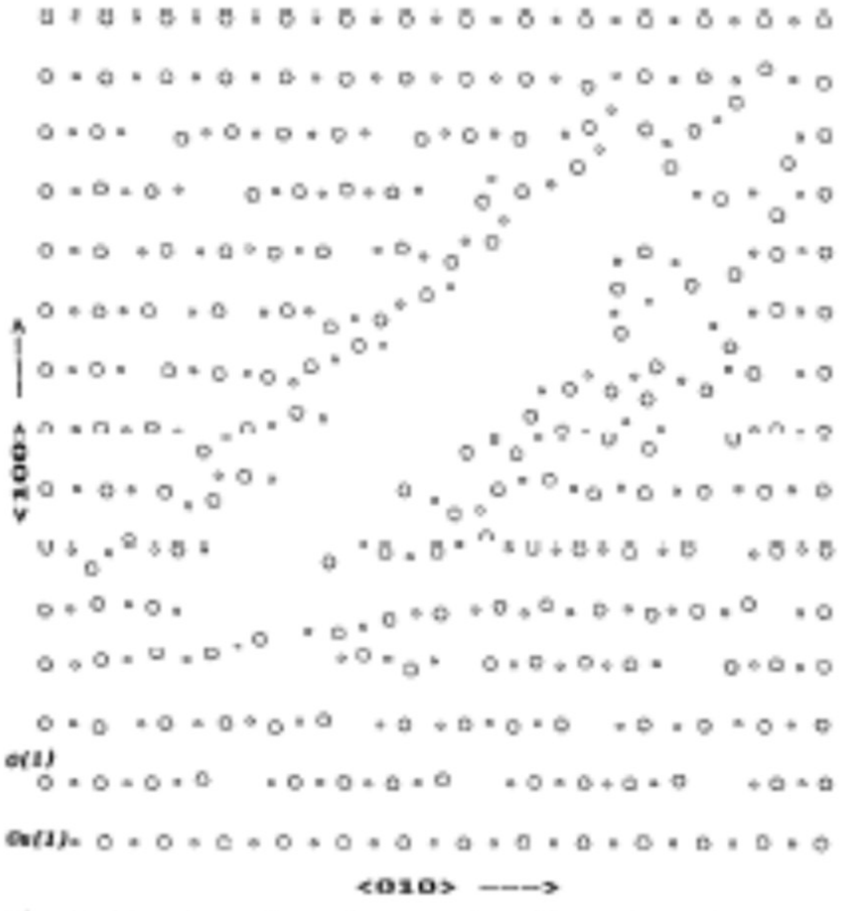

Fig 18: 500 eV O1 pka in $YBa_2Cu_3O_7$ (Cui *et al*. Nucl. Instrum. Methods Phys. Res. B 91 (1994) 374–7).

Previous cascades in $YBa_2Cu_3O_7$

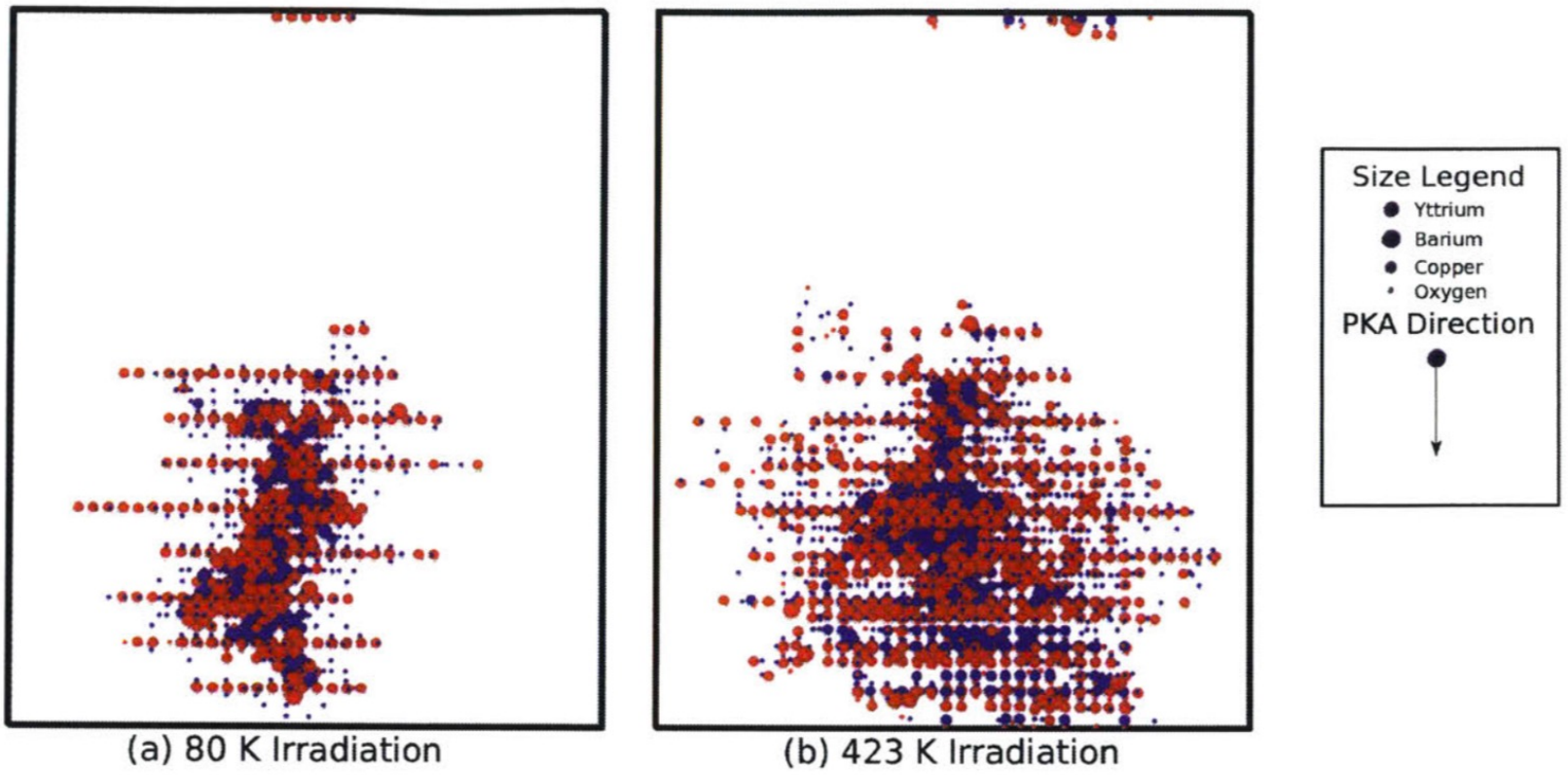

Fig 19: Comparison of 80 K (left) and 423 K 10 keV (right) from MD simulations (Sorbom PhD Thesis 2017).

A potential problem

- If we explore the charges on the ions more closely we can see that to achieve charge neutrality the Cu ions must take both the +2 and +3 charge states.
- As charges are assigned at the start of the simulation, if a Cu ion switches sites during the damage process we will end up with a Cu^{+3} ion on a Cu^{+2} site and vice versa.

Derive a new potential

- New potential fitted to properties derived from DFT:
  - Lattice parameters
  - Elastic Constants
  - Thermal Expansion
  - Ensure no negative phonons

- Potential fitted using a combination of a ‘particle swarm’ and a Nelder Mead Simplex in the PProFit package.

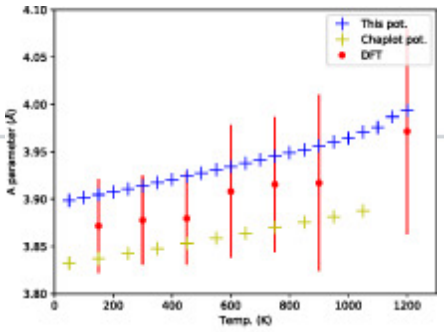

(a)

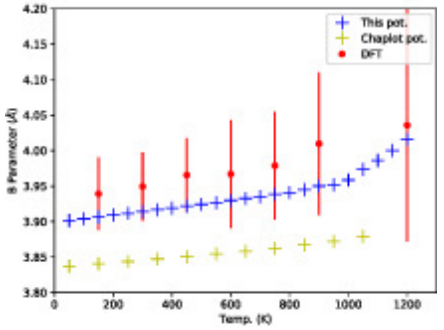

(b)

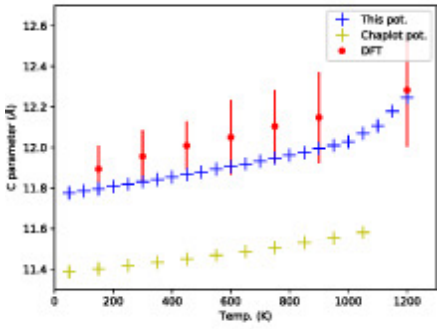

(c)

Fig 20: Plots of lattice parameters as a function of temperature compared to AIMB.

Intrinsic defect processes

Lancaster University

Reaction energies for the intrinsic defect processes in $YBa_2Cu_3O_7$ (Normalised per defect)

Reaction	Potential /eV	DFT /eV
$O_O \rightarrow O_i + V_O$	**0.48**	**0.49**
$Y_Y \rightarrow Y_i + V_Y$	5.65	4.46
$Ba_{Ba} \rightarrow Ba_i + V_{Ba}$	4.59	3.86
$Cu_{Cu} \rightarrow Cu_i + Cu_Y$	2.79	3.08
$Y_Y + Ba_{Ba} \rightarrow Ba_Y + Y_{Ba}$	*1.04*	*0.76*
$Y_Y + Cu_{Cu} \rightarrow Cu_Y + Y_{Cu}$	2.27	1.69
$Cu_{Cu} + Ba_{Ba} \rightarrow Ba_{Cu} + Cu_{Ba}$	2.16	2.07

Some notable differences

Lancaster University

Comparison of oxygen vacancy defects

Site	Potential /eV	DFT /eV
O1	10.30	**1.01**
O2	**9.45**	1.6
O3	**9.38**	1.71
O4	10.34	**0.88**

Some notable differences

Comparison of oxygen interstitial defects

Site	Potential /eV	DFT /eV
1	-6.74	2.14
2	**-8.42**	0.26
3	-1.57	2.27
4	-3.34	0.27
5	-5.51	**0.11**
6	-1.15	**0.1**
7	-0.99	**0.11**

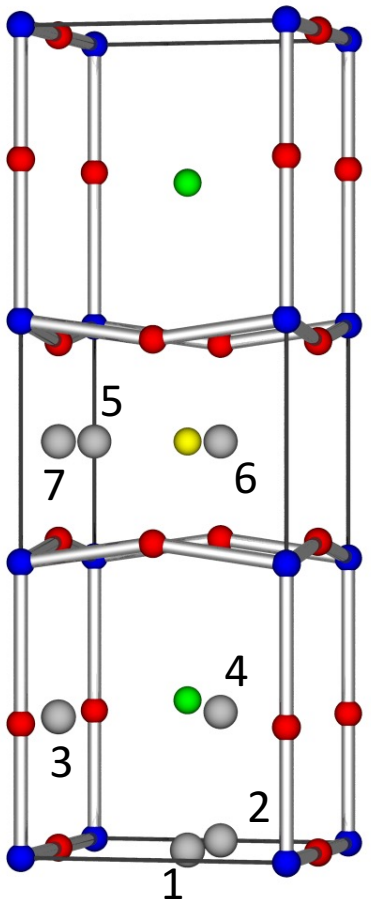

Fig 10: Interstitial sites in $YBa_2Cu_3O_7$.

Threshold Displacement Energies

Lancaster University

- Threshold displacement energies demonstrate a wide distribution:

Comparison of oxygen interstitial defects

	X	Y	Z	xy	yz	yz
O1	9.14	12.95	15.11	17.43	19.92	15.11
O2	12.95	25.39	12.95	25.39	15.11	67.34
O3	15.11	12.95	12.95	17.43	25.39	17.43
O4	15.11	17.43	38.32	15.11	2.5	22.57
Cu1	9.96	9.96	23.79	13.91	6.67	
Cu2	9.96	29.72	29.72	36.31	9.96	13.91
Ba	78.46	30.07	51.42	4.45	51.42	30.07
Y	33.28	33.28	50.80	33.28	41.58	41.58

Threshold Displacement Energies

- Given the importance of the threshold displacement energies we have a project to explore these using *ab initio* MD.

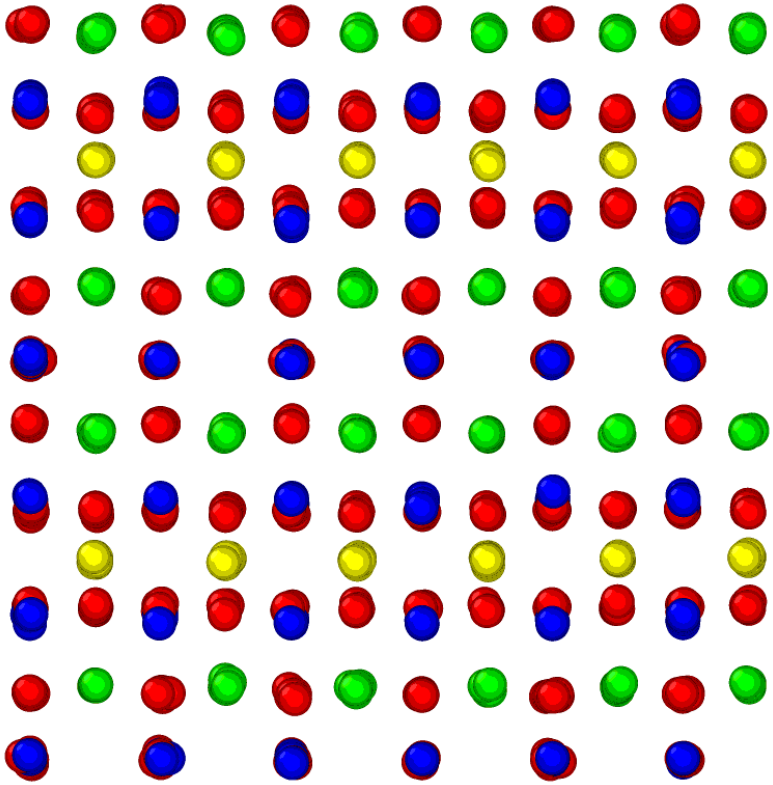

Fig 21: 30 eV displacement of an oxygen ion.

Radiation damage cascade

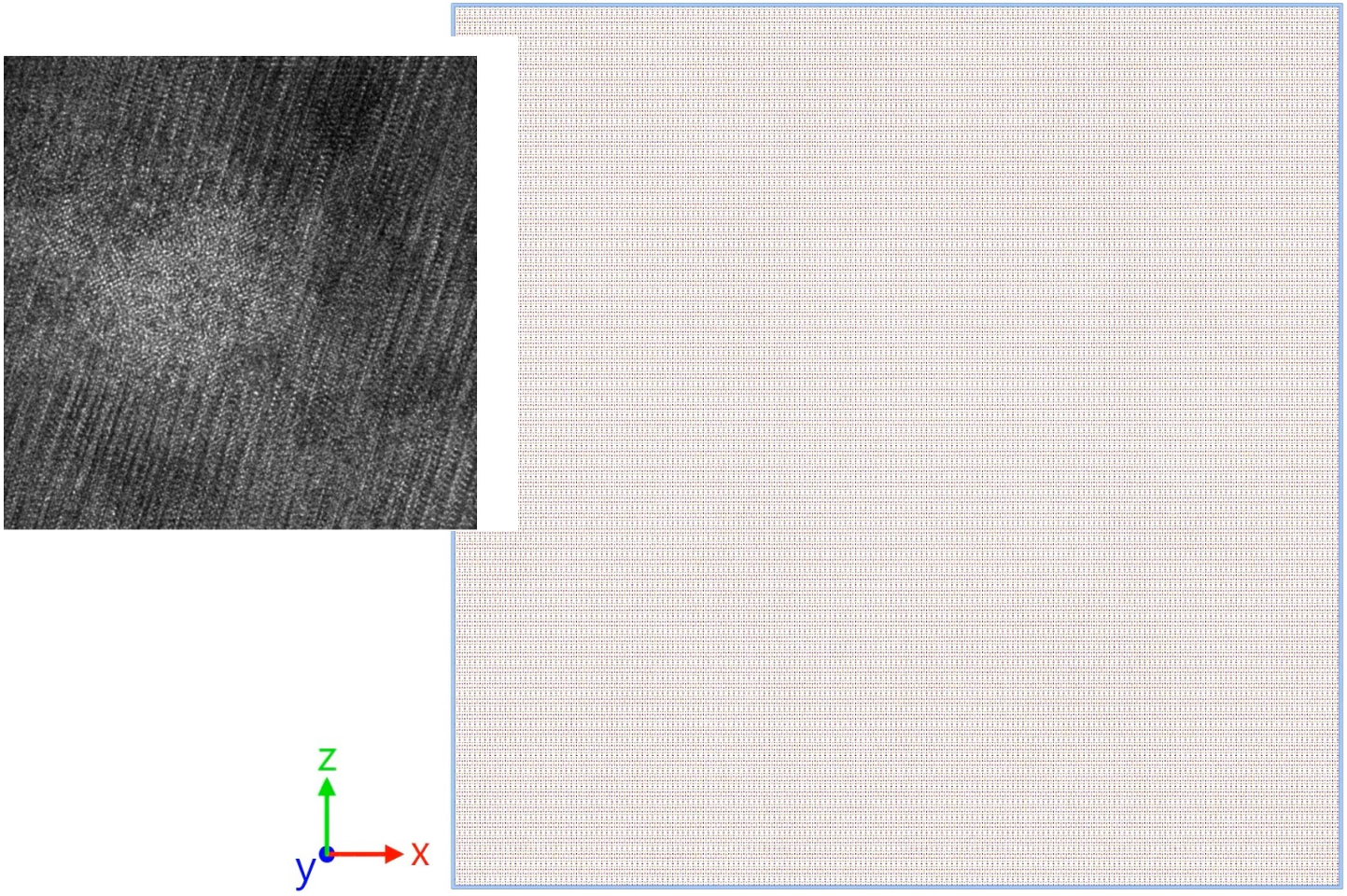

Fig 22: A Ba cascade in $YBa_2Cu_3O_7$.

Radiation damage cascades

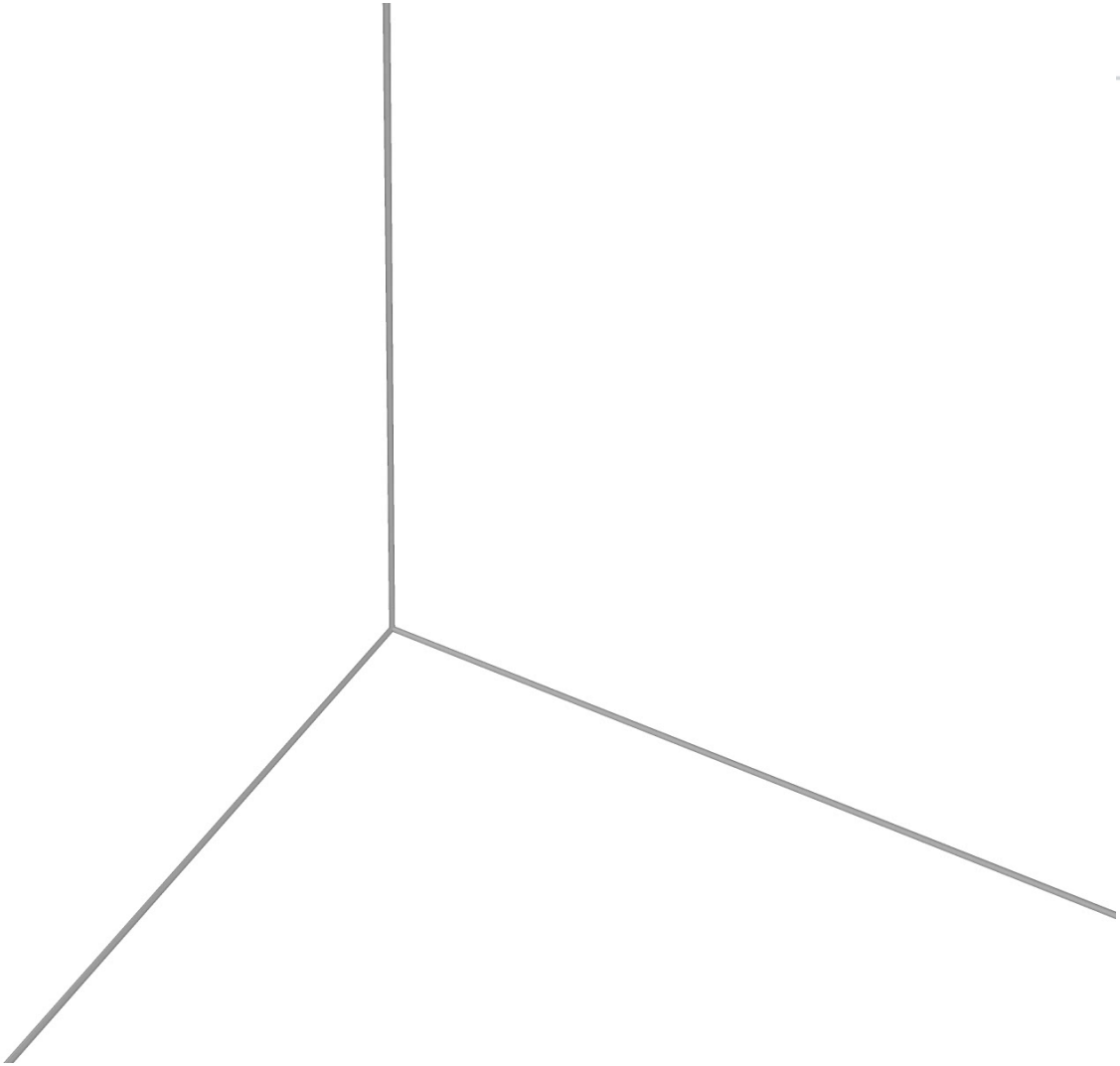

Fig 23: Evolution of a 50 keV Ba pka.

Radiation damage cascades

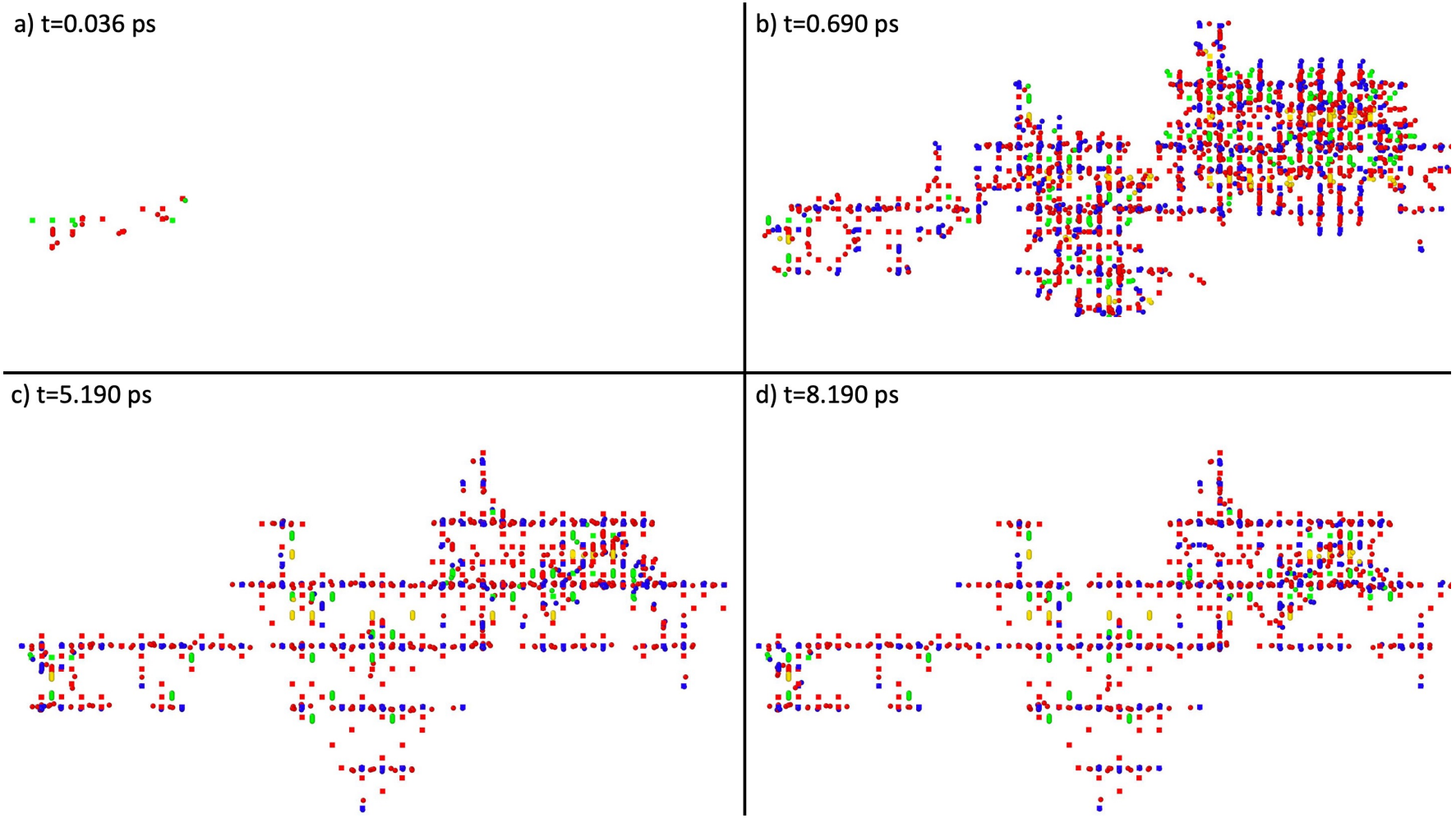

Fig 24: Snapshots of a 5 keV Ba pka in $YBa_2Cu_3O_7$.

Radiation damage cascades

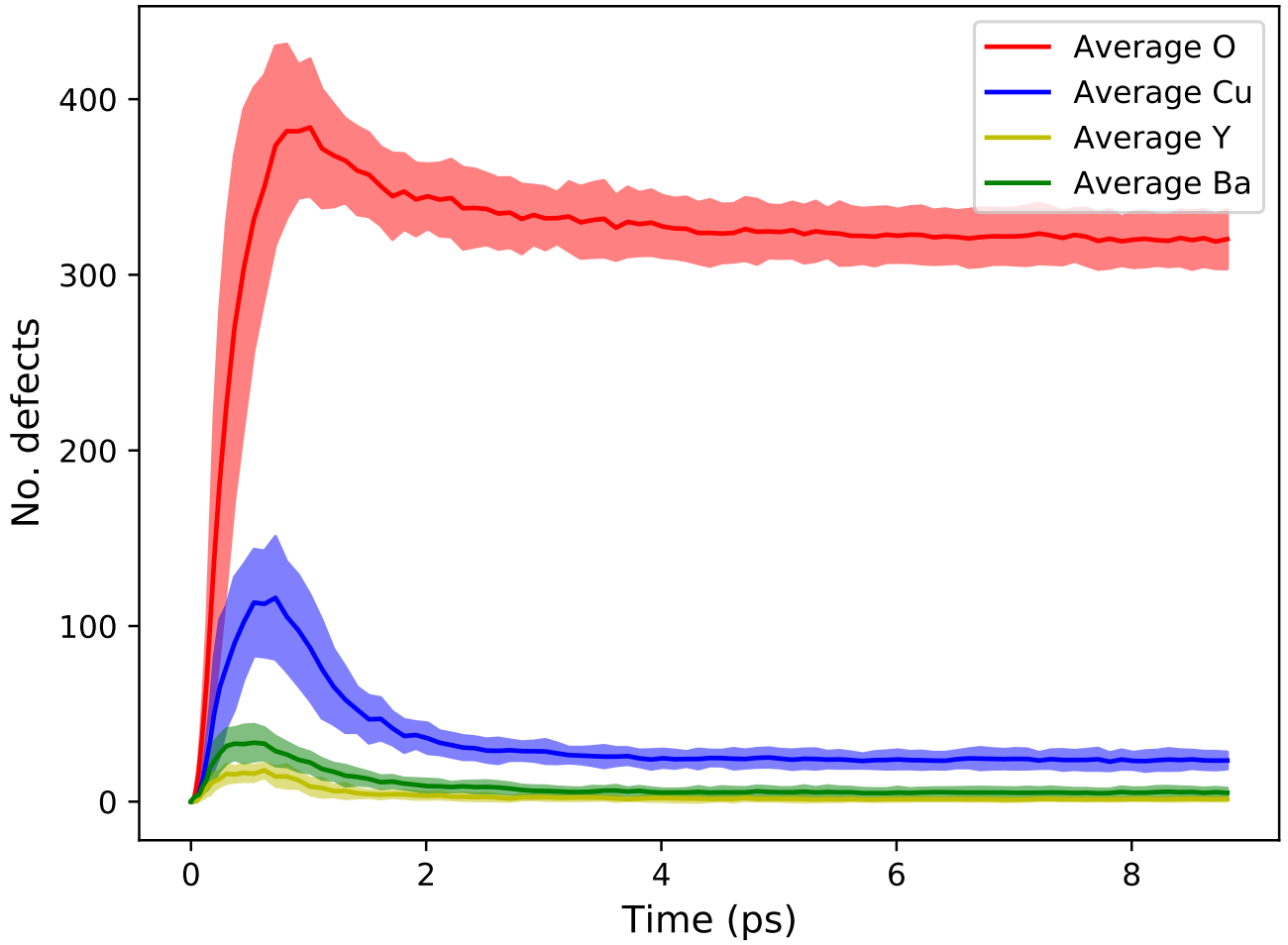

Fig 25: Number of vacancy defects by species as a function of time in $YBa_2Cu_3O_7$.

Radiation damage cascades

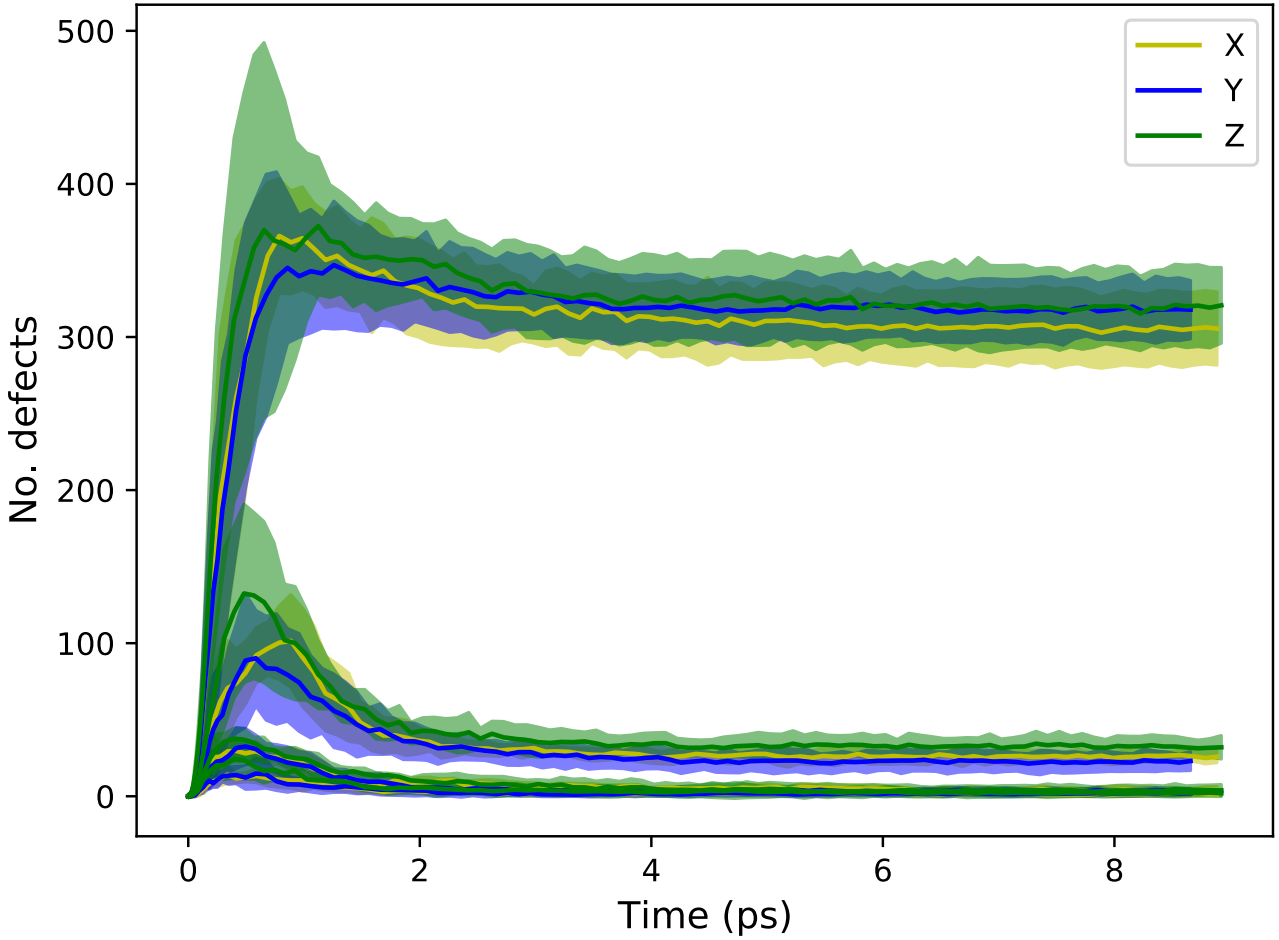

Fig 26: Number of vacancy defects as a function of time for different directions $YBa_2Cu_3O_7$.

Radiation damage cascades

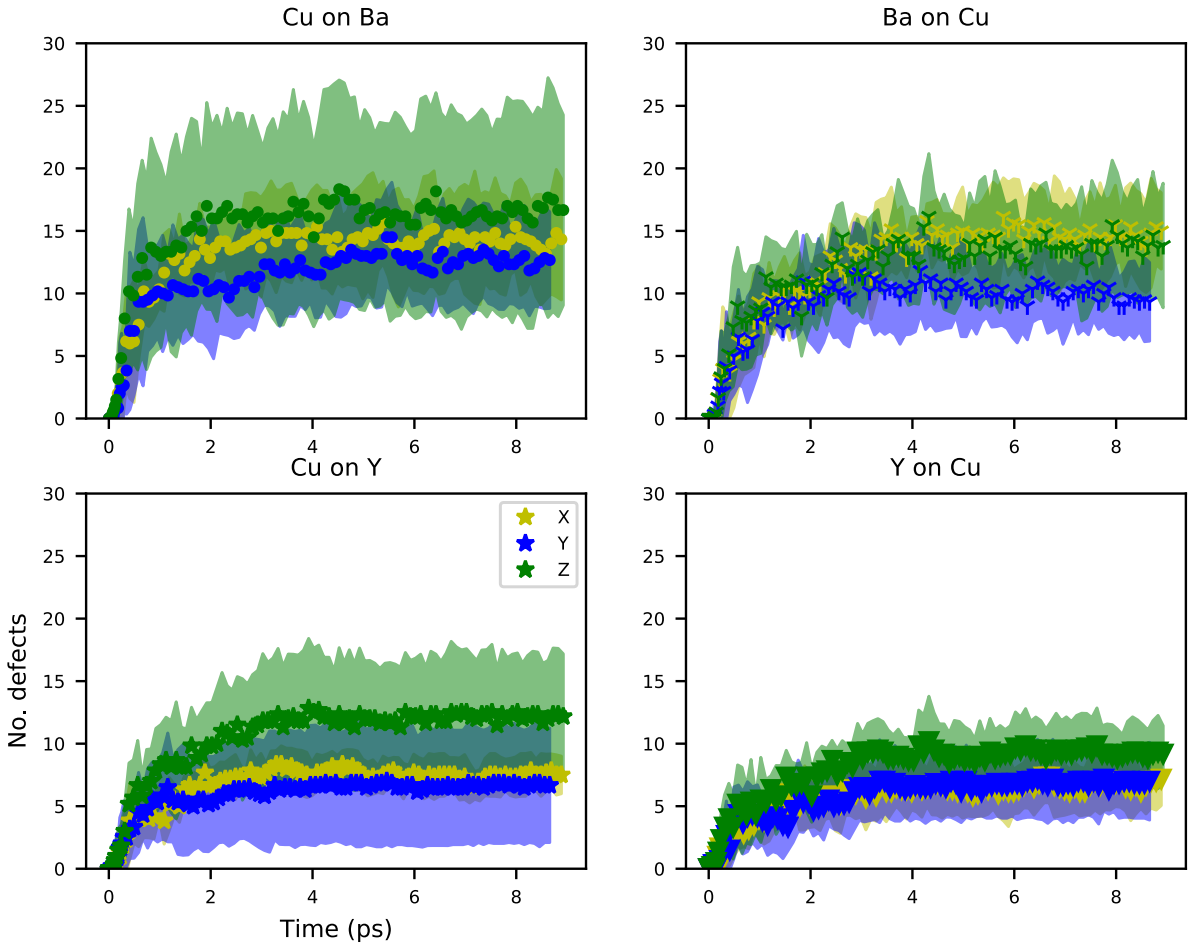

Fig 27: Number of antisite defects as a function of time for different directions $YBa_2Cu_3O_7$.

Radiation damage cascades

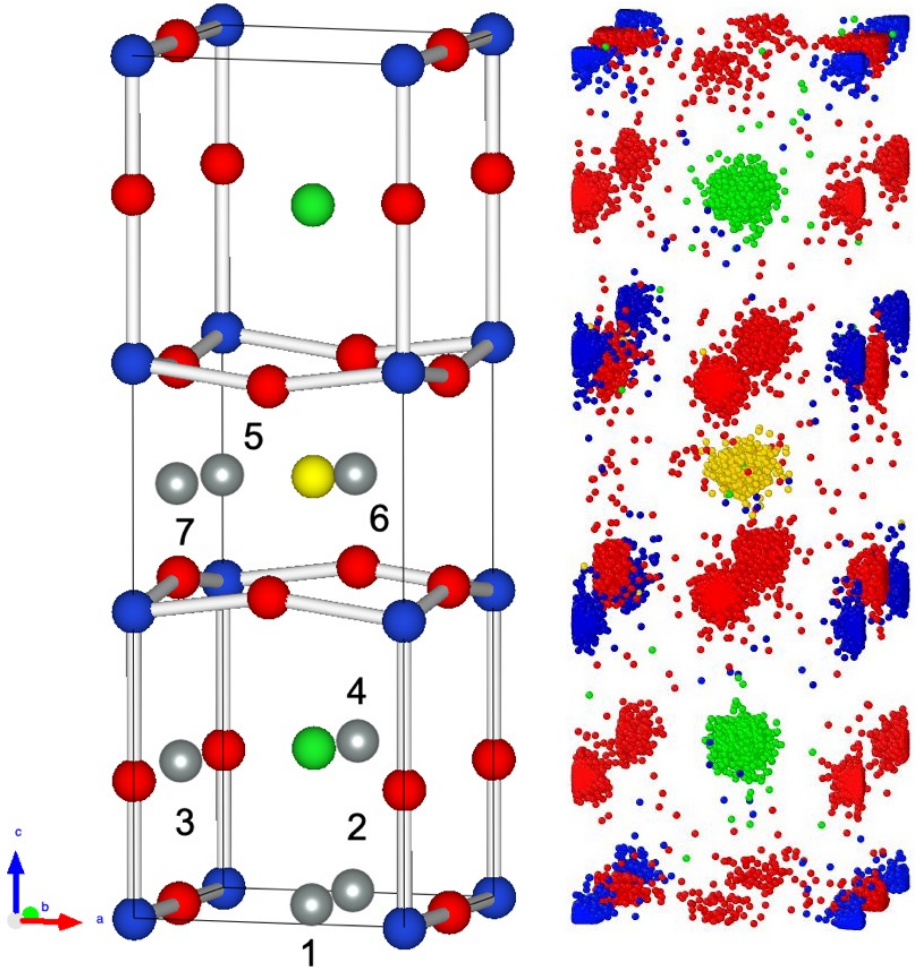

Fig 28: Atom positions folded back into the unitcell at 5.4 ps during a 5 keV cascade at 25 K.

Radiation damage cascades

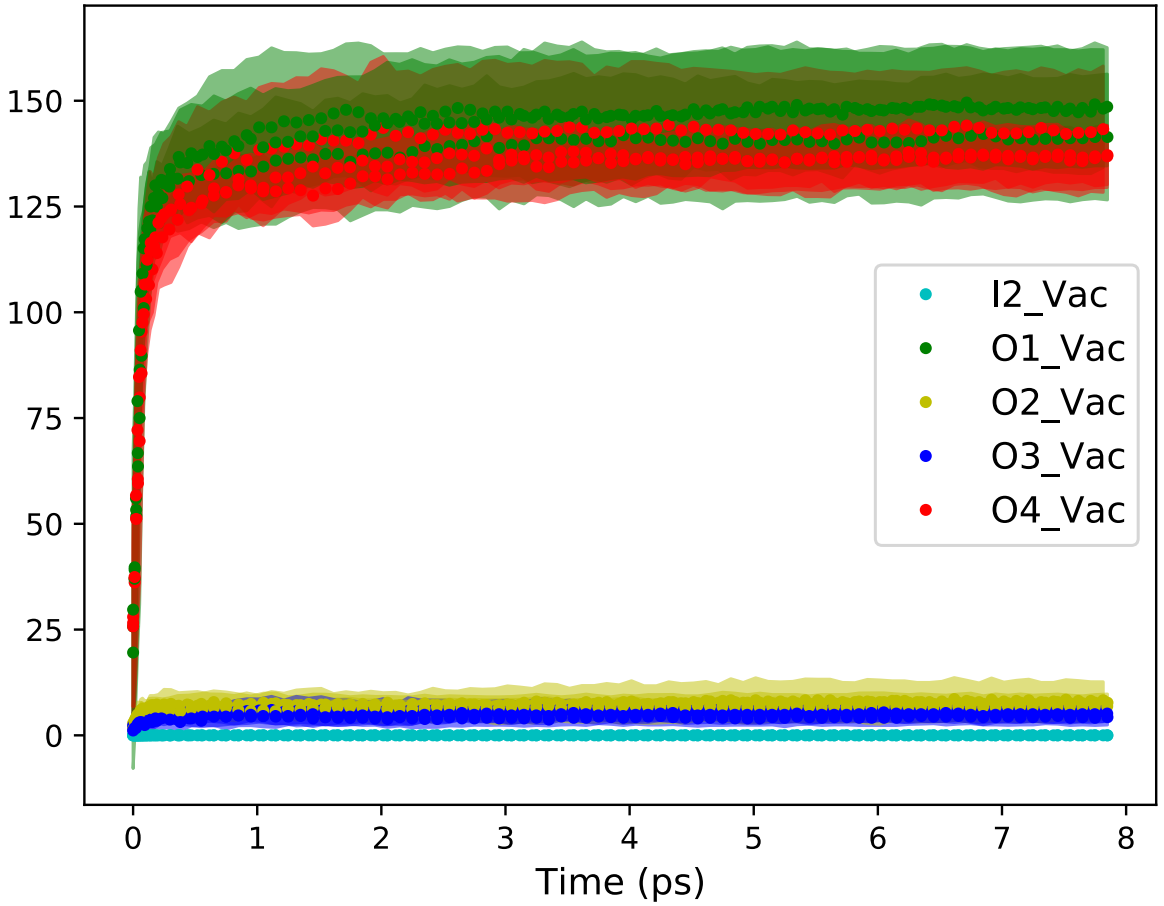

Fig 29: Location of starting positions of atoms found on the interstitial 2 site.

Radiation damage cascades

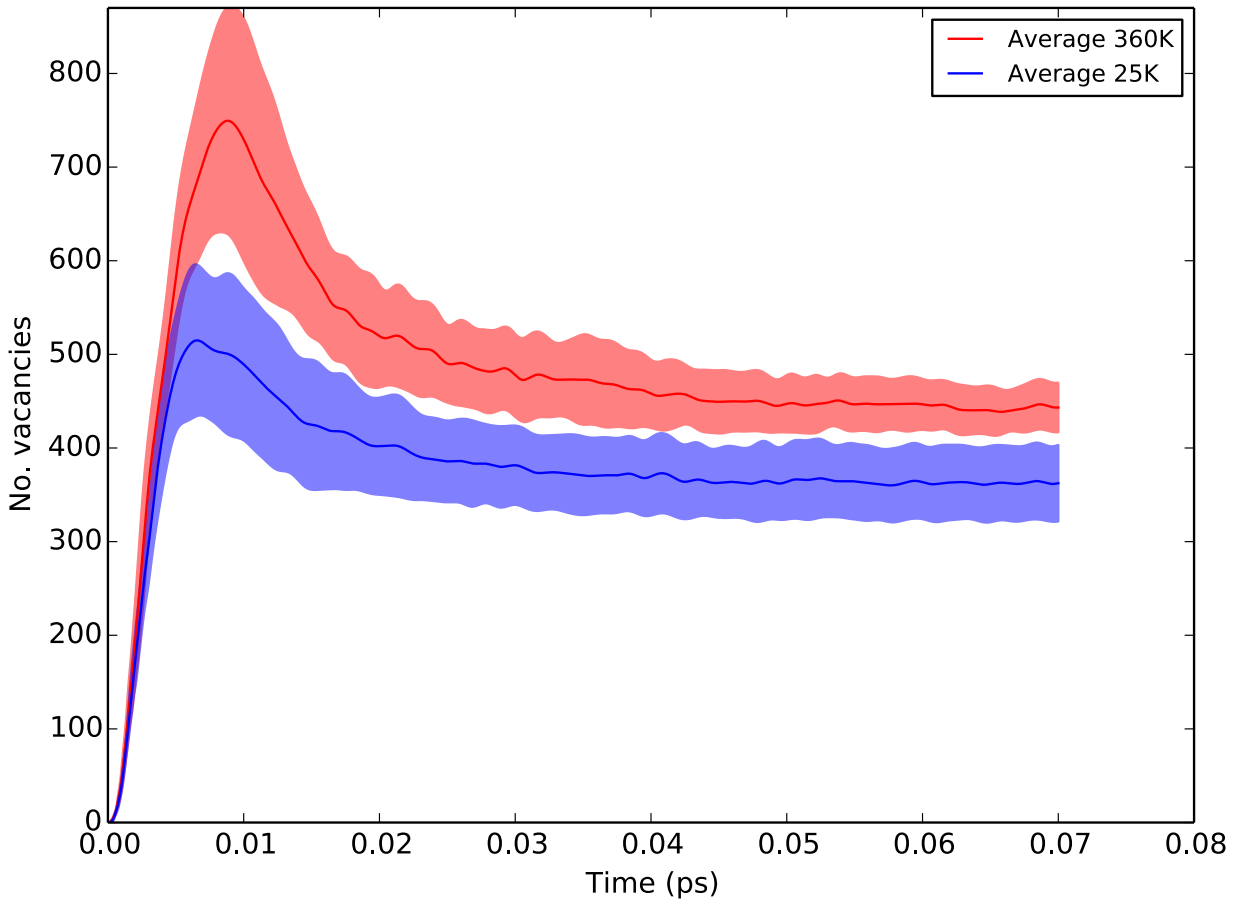

Fig 30: Number of vacancy defects created at different temperatures.

Oxygen diffusion

Annealed at 300 K

25 K cascade

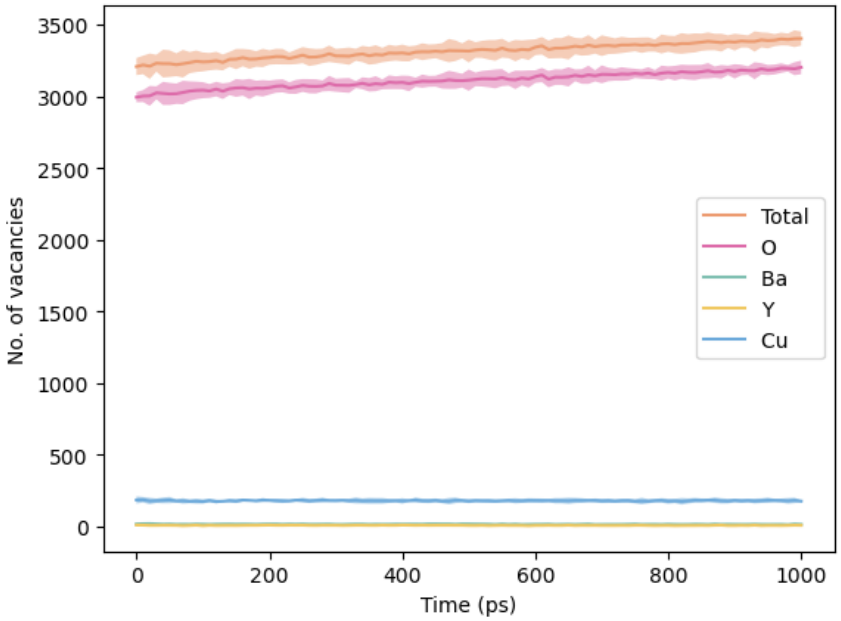

360 K cascade

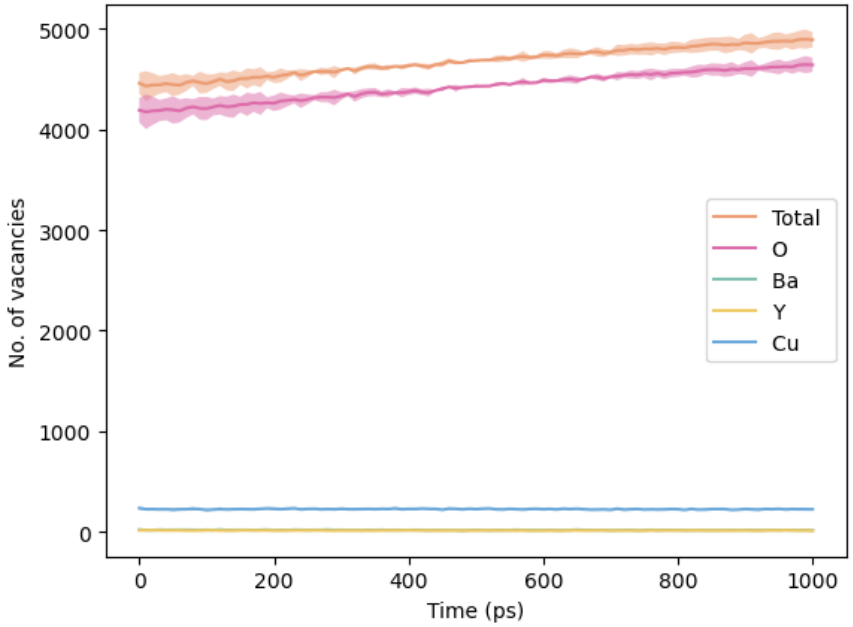

Fig 31: Showing the number of vacancies as a function of time for 25 K and 360 K cascades annealed at 300 K. Data averaged over two data sets with standard deviation shown as shaded region.

Vacancies annealed for each temperature of damage cascade

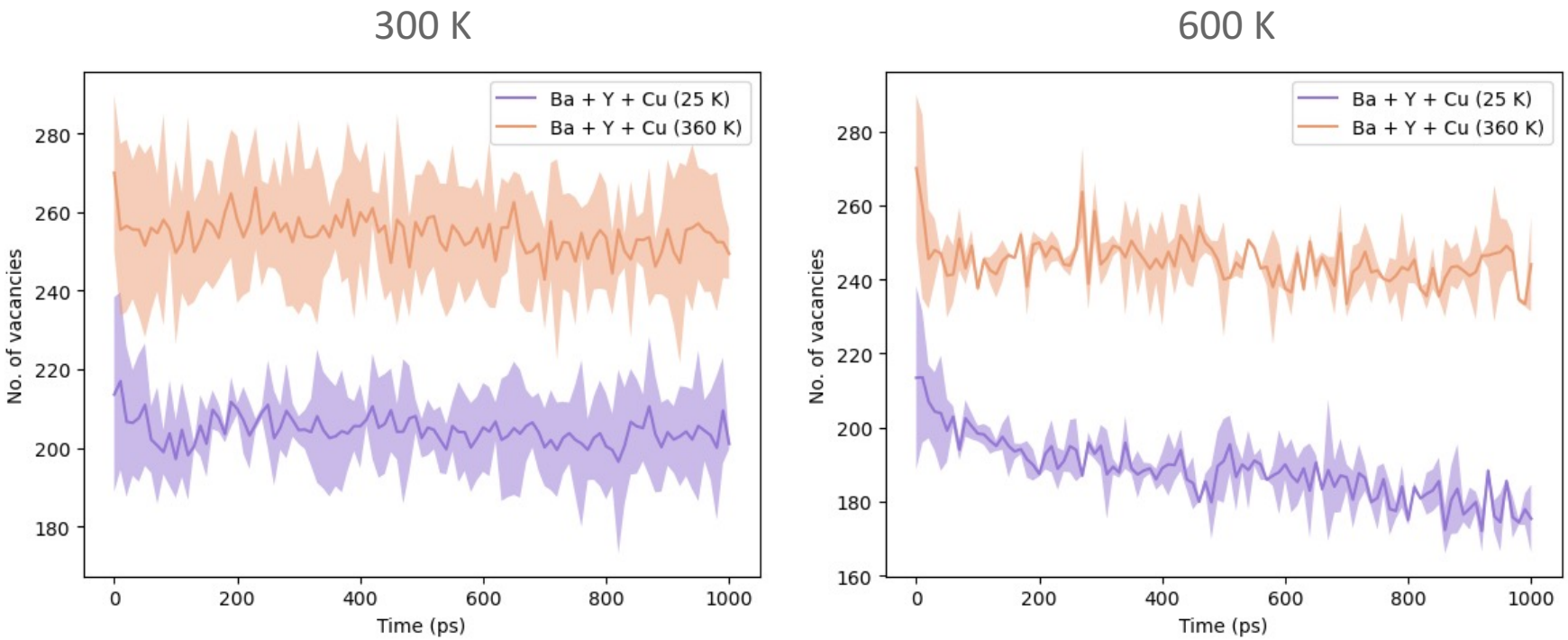

Fig 32. Showing the number of total Ba, Y, and Cu vacancies as a function of time for 25 K and 360 K cascades annealed at 300 K and 600 K. Data averaged over two data sets with standard deviation shown as shaded region.

Vacancies per type for 25 K cascade annealed at 600 K

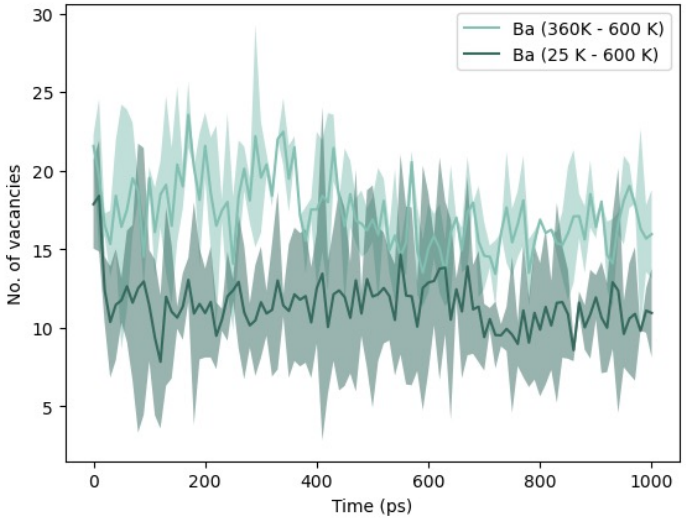

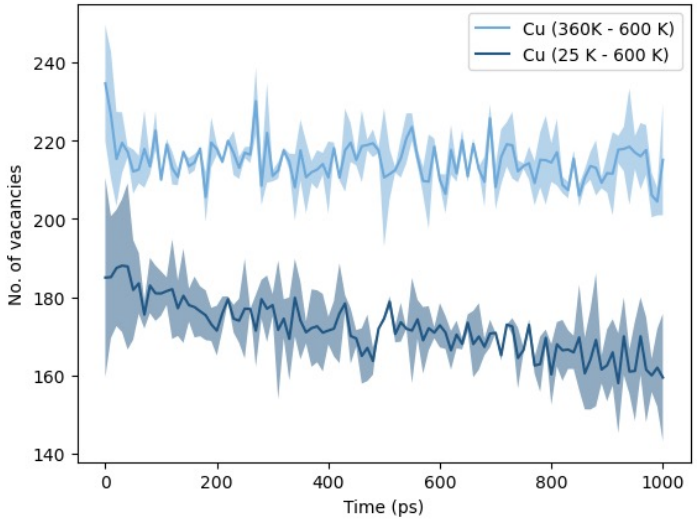

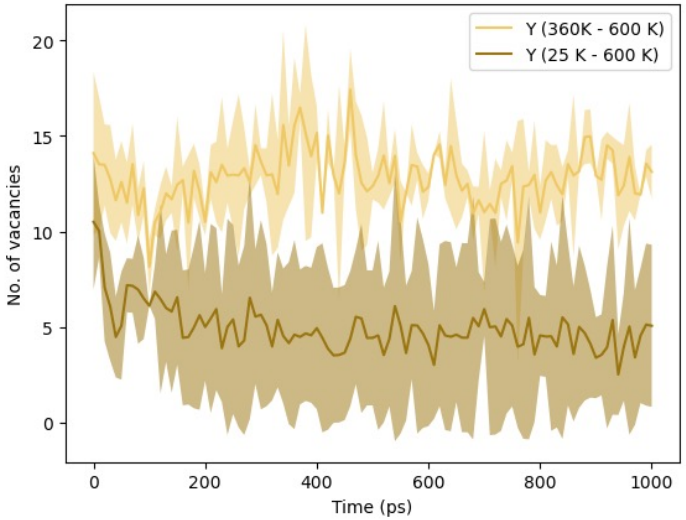

Fig 32: Showing the number of total Ba, Y, and Cu vacancies as a function of time for 25 K and 360 K cascades annealed at 600 K. Data averaged over two data sets with standard deviation shown as shaded region.

Summary

- Defect chemistry dominated by oxygen vacancy defects.
- Antisite defect processes have relatively low energies, which suggests they are relatively common.
- Developed a new potential for use in MD simulations that allows Cu to switch between the Cu1 and Cu2 sites without consequence.
- Cascades result in an amorphous core surrounded by planar Cu and O defect rich regions.
- Very low levels of defect recombination.
- Population of interstitial 2 site and vacancy defects in the nearby oxygen 1 and 4 sites, means the planar regions are in the CuO-chains.
- Remnant defect population NOT dictated by thermodynamics.
- More remnant defects in simulations at 360 K than 25 K.
- We see some recombination of cations from cascades performed at low temperature that is not evident if the cascade occurred at high temperature.

Many thanks to everyone for their attention!

Lancaster University

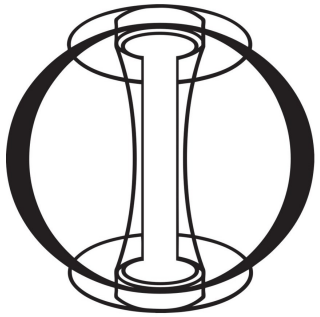

tokamak energy

UK Atomic Energy Authority

EPSRC

archer2

Vacancy count per type

Annealed at 300 K

25 K cascade

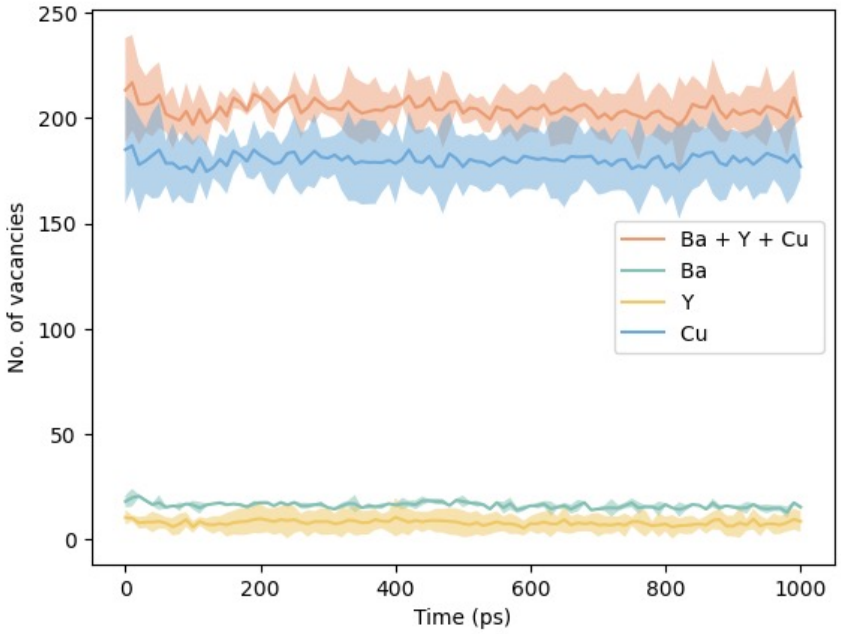

360 K cascade

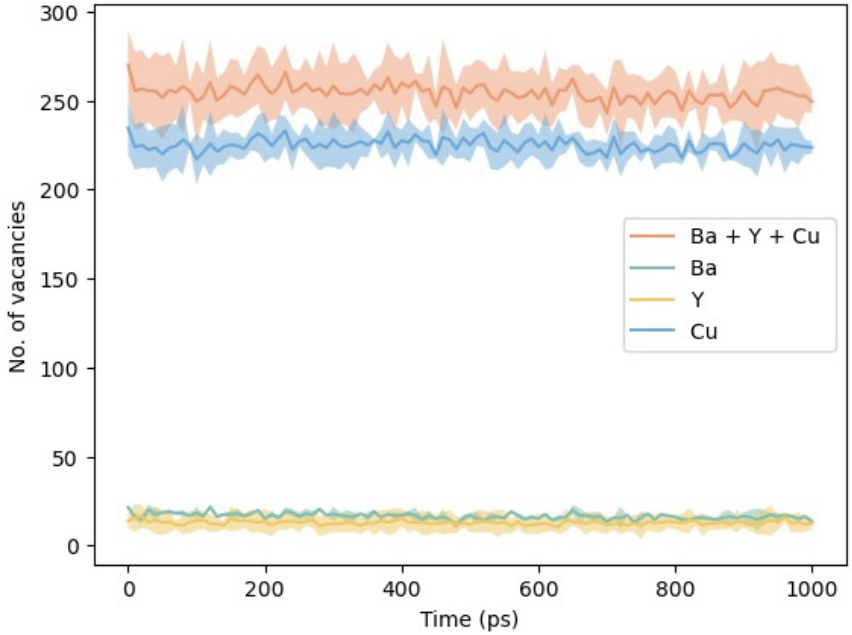

Fig 32: Showing the number of vacancies per particle type (Ba, Y, and Cu) as a function of time for 25 K and 360 K cascades annealed at 300 K. Data averaged over two data sets with standard deviation shown as shaded region.

Radiation damage cascades

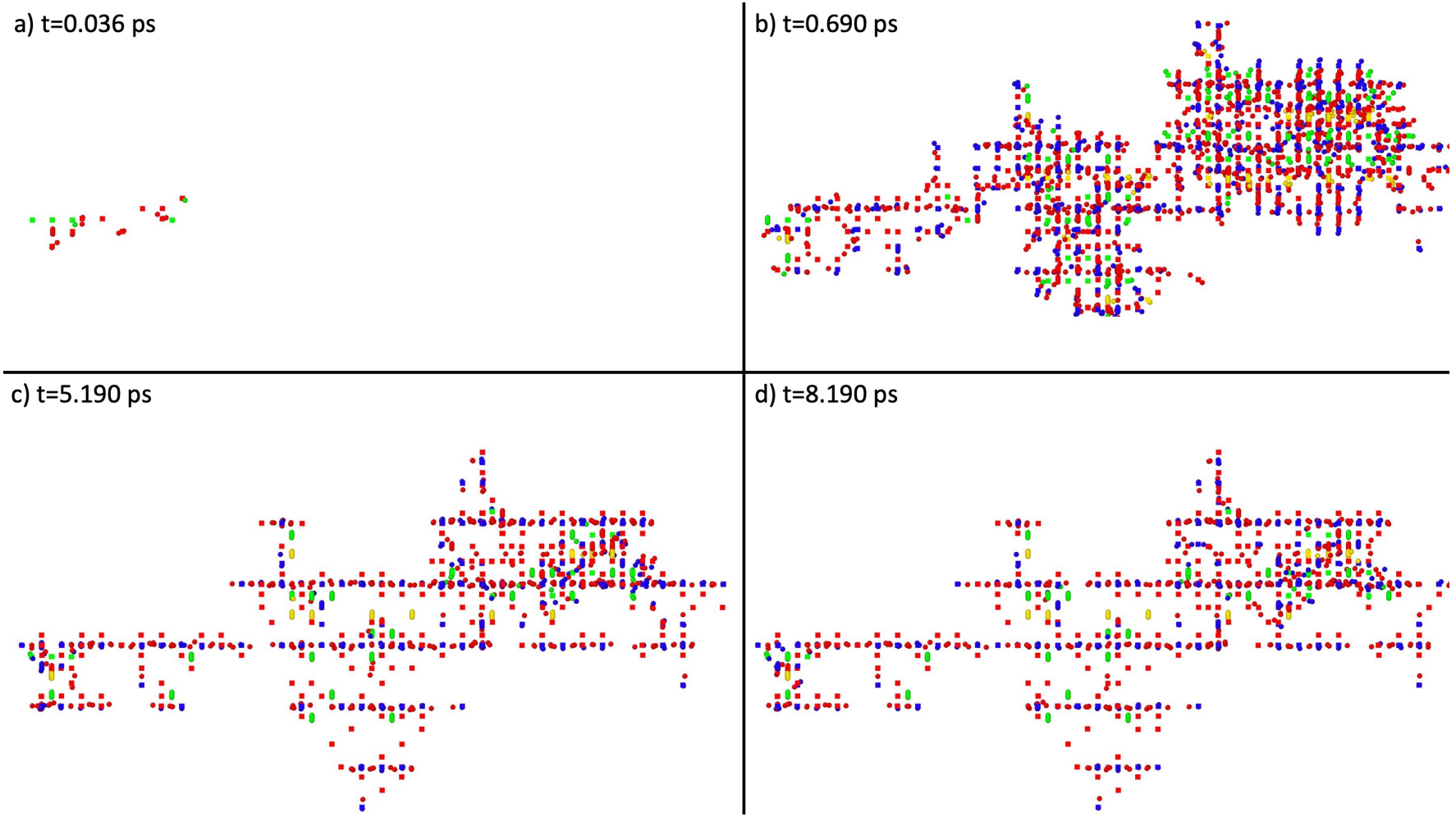

Fig 13: Snapshots of a 5 keV Ba pka in $YBa_2Cu_3O_7$.

Radiation damage cascades

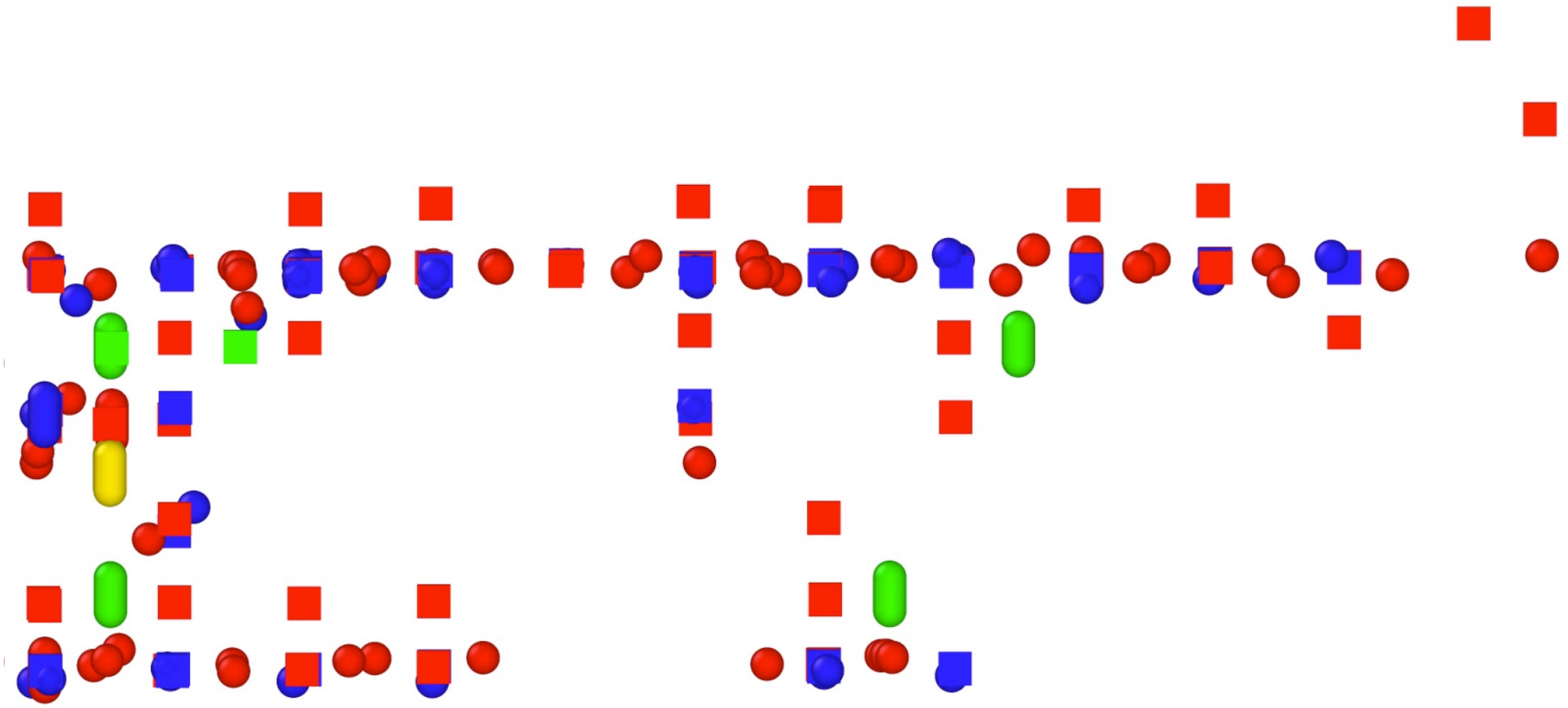

Fig 14: Extended defect region in the CuO-chain.

Radiation damage in HTS materials

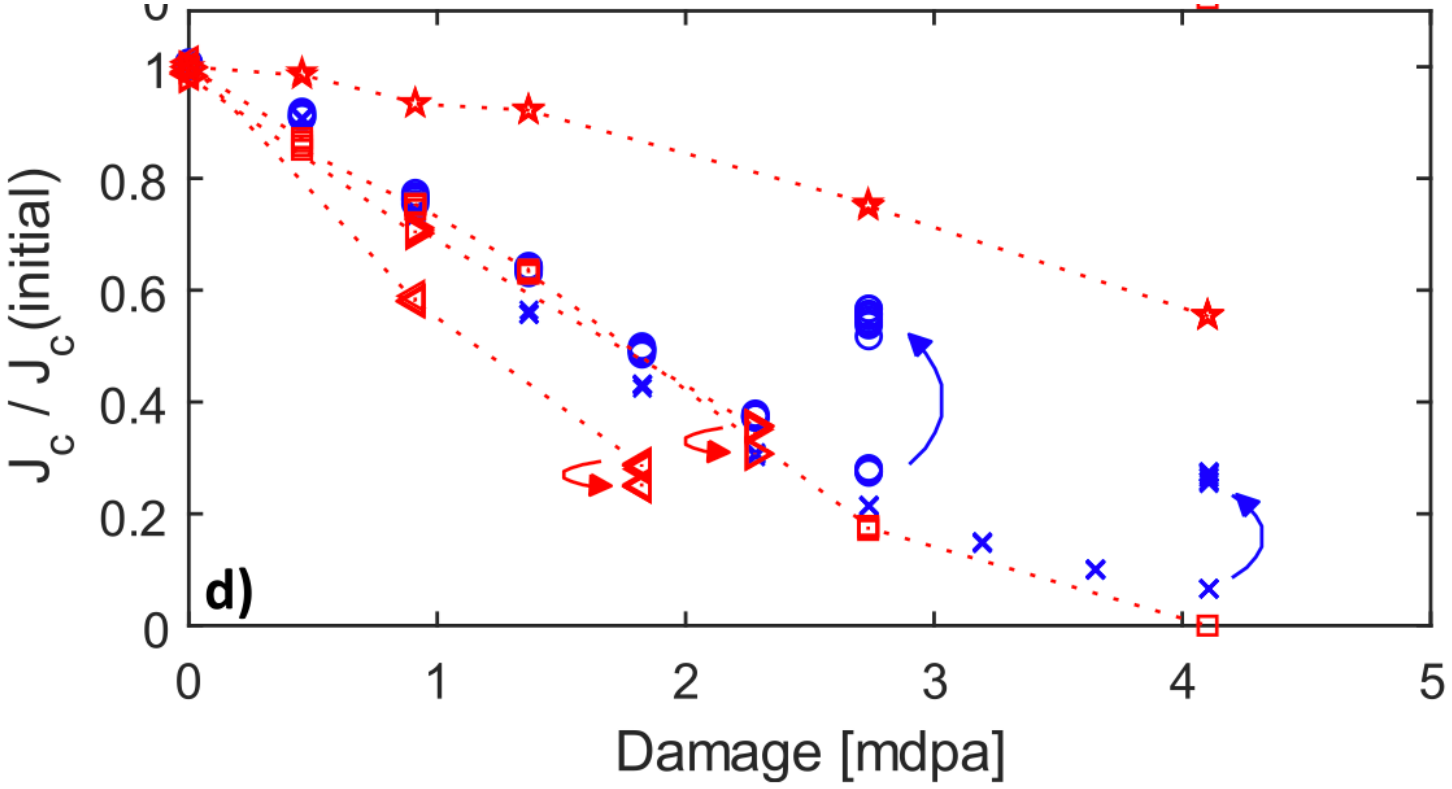

Fig 4: Plot showing the reduction in critical current with He irradiation at room temperature (red) and operational temperature (blue) (Iliffe *et al*. SUST 34 (2021) 09LT01).